AD-A044 028 ARMY MISSILE RESEARCH AND DEVELOPMENT COMMAND REDSTO--ETC F/G 1/3
AEROBALLISTIC STUDY OF AN ATTACK MINI-RPV.(U)
JUL 77 R B POWELL, D W HOLDER, R E DICKSON

UNCLASSIFIED DRDMI-TD-77-16 NL

1 OF 1
AD A044028

END
DATE FILMED
10-77
DDC

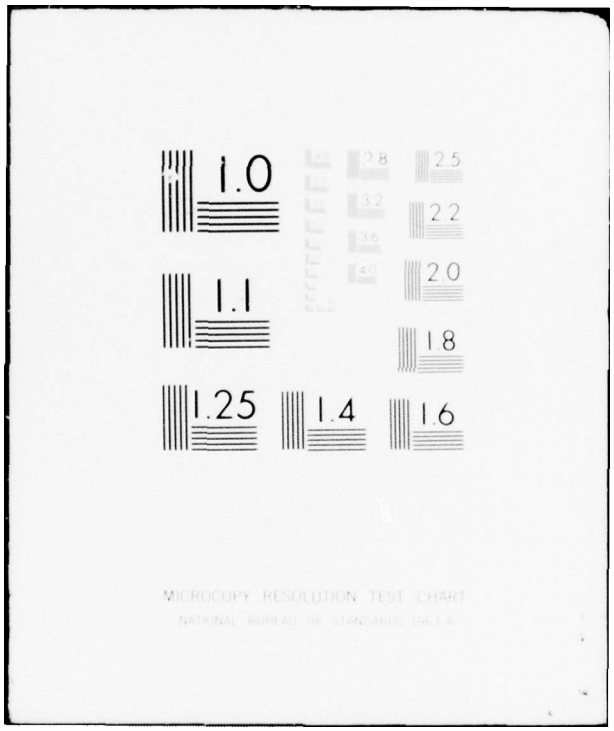
1.0
1.1
1.25
1.4
1.6
2.8
2.5
3.2
2.2
3.6
2.0
4.0
1.8
MICROCOPY RESOLUTION TEST CHART
NATIONAL BUREAU OF STANDARDS 1963 A

U.S. ARMY MISSILE RESEARCH AND DEVELOPMENT COMMAND

Redstone Arsenal, Alabama 35809

12
B.S.

TECHNICAL REPORT TD—77—16

AEROBALLISTIC STUDY OF AN ATTACK MINI-RPV

Aeroballistic Directorate
Technology Laboratory

13 July 1977

Approved for public release; distribution unlimited

DISPOSITION INSTRUCTIONS

DESTROY THIS REPORT WHEN IT IS NO LONGER NEEDED. DO NOT RETURN IT TO THE ORIGINATOR.

DISCLAIMER

THE FINDINGS IN THIS REPORT ARE NOT TO BE CONSTRUED AS AN OFFICIAL DEPARTMENT OF THE ARMY POSITION UNLESS SO DESIGNATED BY OTHER AUTHORIZED DOCUMENTS.

TRADE NAMES

USE OF TRADE NAMES OR MANUFACTURERS IN THIS REPORT DOES NOT CONSTITUTE AN OFFICIAL INDORSEMENT OR APPROVAL OF THE USE OF SUCH COMMERCIAL HARDWARE OR SOFTWARE.

UNCLASSIFIED

SECURITY CLASSIFICATION OF THIS PAGE (When Data Entered)

REPORT DOCUMENTATION PAGE

READ INSTRUCTIONS BEFORE COMPLETING FORM

1. REPORT NUMBER: TD-77-16
2. GOVT ACCESSION NO.:
3. RECIPIENT'S CATALOG NUMBER:

4. TITLE (and Subtitle): "AEROBALLISTIC STUDY OF AN ATTACK MINI-RPV"

5. TYPE OF REPORT & PERIOD COVERED: Technical Report

6. PERFORMING ORG. REPORT NUMBER: TD-77-16

7. AUTHOR(s): Rex B. Powell, Donald W. Holder, and Richard E. Dickson

8. CONTRACT OR GRANT NUMBER(s):

9. PERFORMING ORGANIZATION NAME AND ADDRESS:
Commander
US Army Missile Command
Attn: DRDMI-TD
Redstone Arsenal, Alabama 35809

10. PROGRAM ELEMENT, PROJECT, TASK AREA & WORK UNIT NUMBERS:
DA 1L362303A214
AMCMS No 632303.2140511

11. CONTROLLING OFFICE NAME AND ADDRESS:
Commander
US Army Missile Command
Attn: DRDMI-TI
Redstone Arsenal, Alabama 35809

12. REPORT DATE: 13 July 1977

13. NUMBER OF PAGES: 81

14. MONITORING AGENCY NAME & ADDRESS (if different from Controlling Office):

15. SECURITY CLASS. (of this report): UNCLASSIFIED

15a. DECLASSIFICATION/DOWNGRADING SCHEDULE:

16. DISTRIBUTION STATEMENT (of this Report)

Approved for public release; distribution unlimited.

17. DISTRIBUTION STATEMENT (of the abstract entered in Block 20, if different from Report)

18. SUPPLEMENTARY NOTES

410 126

19. KEY WORDS (Continue on reverse side if necessary and identify by block number)

Remotely piloted vehicle
Electrooptical simulation system
Target hit probability
Man modeling
Man/machine simulation

20. ABSTRACT (Continue on reverse side if necessary and identify by block number)

This report presents the results of an aeroballistic study of an attack mini-RPV. The work was performed by the Aeroballistics Directorate during the period from January 1972 to January 1976.

DD FORM 1 JAN 73 1473 EDITION OF 1 NOV 65 IS OBSOLETE

UNCLASSIFIED

SECURITY CLASSIFICATION OF THIS PAGE (When Data Entered)

CONTENTS

FOREWORD

The contents of this report constitute the lecture notes prepared for the Von Karman Institute for Fluid Dynamics lecture series "Remotely Piloted Vehicles — Aerodynamics and Related Topics," 23-27 May 1977. The lecture entitled "Feasibility Study of a Mini-RPV for Attack" was presented by Mr. Rex B. Powell on 26 May 1977 at the Von Karman Institute. Copies of these notes were supplied by Von Karman Institute to the lecture attendees. The work leading to this report was conducted by the Aeroballistics Directorate. Technology Laboratory, US Army Missile Research and Development Command, during the period from January 1972 to January 1976. This work covered, in detail, many aspects and subsystems of an attack remotely piloted vehicle system; however, only those items related to aeroballistics are including for purposes of this report.

I. SYSTEM CONSIDERATIONS

A. Introduction

In the United States, the Army's use of remote piloted vehicles (RPV's) began in the mid-50's with the development of a series of vehicles for battlefield surveillance and target acquisition. These vehicles were designed primarily to support the tactical missiles in and planned for field use. For various reasons, this series of RPV's was not extremely successful. The first and only fielded RPV of the series had significant flight control and maintenance problems and imposed unnecessary burdens on the field commanders. The second RPV of the series was designed to circumvent the problems of the system while the third and fourth systems of the series were aimed at increased capability. The requirement changes and improvements attempted during the development phase caused excessive cost growth and in the late-60's all programs were terminated.

These efforts toward utilization of RPV's were rather disappointing to the research and development (R&D) community and to the field commanders who still needed a reliable surveillance and target acquisition capability. Several important lessons were learned from these programs which are valid in beginning any RPV program. These are:

1) Requirements must be realistic with respect to the needs as well as the technology available to satisfy them.

2) Demonstrations to show the feasibility of technical solutions and also allow for user feedback should precede full-scale engineering developments.

3) Adequate level of funding must be programmed; and once a development is started, it should not be continuously modified to avoid cost and schedule overruns.

4) Ease of operation by the troops and minimum maintenance burden are essential.

Today, after a period of inactivity in this field, several things have changed from these early beginnings. The operational needs for reconnaissance, surveillance, and target-acquisition systems are even more acute, since there is a need to complement the progress made in the mobility and

firepower of our forces. Requirements for survivability in a modern air-defense environment and constraints on cost make large, expensive systems unrealistic for tactical Army applications. And a new generation of technology, exemplified by the recent programs in mini-RPV's is exciting a new generation of the Army's user/developer team with potential applications and technological solutions not feasible in the past.

Probably the most significant impetus to recent Army RPV use came from the technological solutions which allowed a substantial reduction in RPV size and weight. With this realization, a review of possible RPV applications to Army missions lead to the identification of the following key applications:

1) Surveillance and designation — Anticipating that in potential future conflicts the forward observer, airborne or on the ground, will be quite vulnerable, and realizing a need for better target-acquisition support for the present firepower elements and future laser-guided weapons, the review recommended as the primary mission application an RPV Designator System. This RPV would perform surveillance and target-acquisition missions within the range of conventional artillery and be able to adjust fire or laser designate for semi-active laser-guided weapons. Such an RPV would clearly have to possess three key features to make it attractive in this role:

a) Survivable in a hostile air-defense environment.

b) Inexpensive.

c) Easily operable by forward troop elements.

2) Over-the-hill surveillance — The field commander continually expresses desire to be able to see over-the-hill, even if he is not able to accurately establish a target location. Such a system is of interest only if it is very cheap and easy to operate and reliable.

3) Electronic warfare — Expendable jammer.

4) Attack RPV — The concept of this RPV is to provide an integrated target acquisition/strike capability by using the on-board sensor information for terminal guidance either through manual or automatic control and by carrying a warhead as part of the useful payload. Such a weapon would have extended point target capability and immediate target damage assessment.

Key features for such an RPV are essentially the same as those required for the surveillance RPV, except, recovery is not required.

The characteristics of all the previously mentioned concepts appeared to be best achieved by the mini-RPV. This can be seen not only from the fact that small RPV's would present smaller vulnerable areas and low observable signatures, but also by the fact that they could be handled by troops without elaborate support equipment. There also seems to be a rule of thumb which states that, after R&D has taken place, vehicles of a given class tend to cost a given amount of dollars per pound.

With this combined surveillance/strike mission in mind, work began to establish the feasibility, capabilities, and limitations of such a device. If given complete freedom, a feasibility program would be designed to:

a) Determine the effectiveness of a small RPV to locate and damage tactical military targets.

b) Define technological problem areas which either prevent concept implementation or require additional work for satisfactory solution.

c) Determine characteristics and impact of the aerodynamic performance parameters on command, control, and mission accomplishment.

d) Provide unit for user testing to form a basis for his evaluation and feedback for design improvement.

In this case, such a comprehensive program was not undertaken but was limited to establishment of preliminary design parameters and investigation of the two recognized significant technical problems of data links and terminal performance with manual tracking.

B. Basic Concept

The basic concept of the attack RPV studied here is shown in Figure 1. The vehicle is launched from a ground based site and flies a mid-course trajectory to the target area. Flight during this period is either under manual or automatic control. In either case, the ground station must track the vehicle and provide position and velocity information. Additionally, a telemetry link provides video data and flight status information, including vehicle heading and altitude. The video data are used to provide a target scene to the operator for target acquisition and target homing after target selection is made.

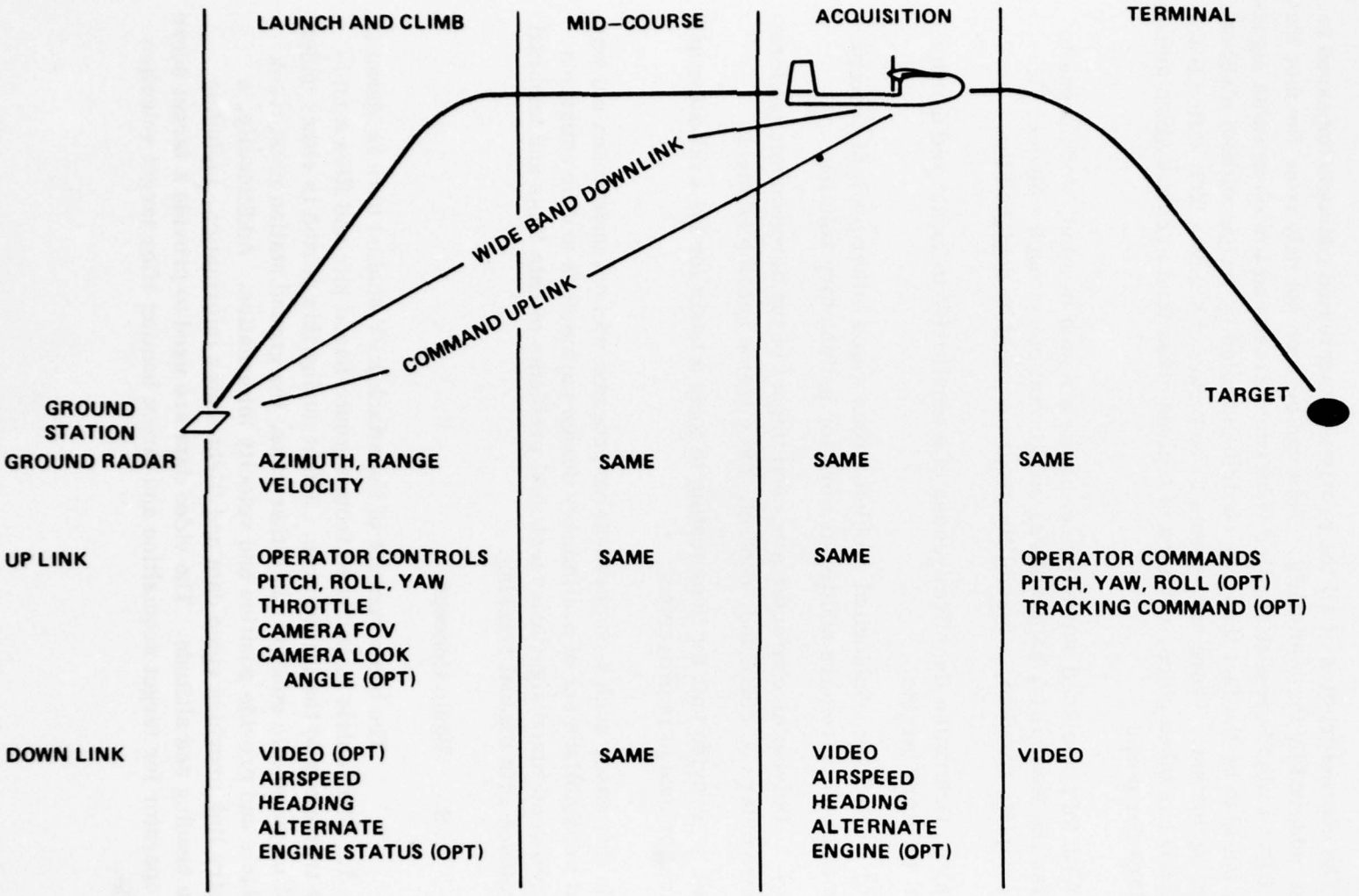

Figure 1. Basic concept.

A number of technical problems are immediately obvious. The first is that such a concept requires a near continuous up and down link to insure a success. This is a difficult requirement when one considers all possible disruptions of the line-of-sight (LOS) and bandwidth requirements. An extensive study was made of the alternatives available for solution to this problem, and several offered a reasonable degree of success. This problem will not be discussed here.

From the onset of this study, cost was a major factor. If the concept was to have merit, it must be less expensive than competitive concepts; therefore, the major thrust was toward the use of unstabilized imaging sensor for both target acquisition and terminal homing. The unstabilized sensor magnifies the problems of interaction of the airframe, operator performance, and ground display. This is the terminal homing problem treated here, both from an analytical and experimental approach, with an effort made to correlate the results.

C. Mini-Attack RPV Cost Effectiveness Considerations

Before a weapon system candidate can be selected to fulfill a military role, a comparative effectiveness of alternative means of meeting the requirement should be conducted, and the cost of developing, producing, and operating the system should also be considered. These cost effectiveness studies should demonstrate a reasonable chance of providing an advance in operational capability at an acceptable cost before development of a system. When compared with other weapon candidates, the selected system should show a lower cost per target kill. Weapon system life cycle costs involve detailed analysis by experts which use well documented methodology and will not be discussed herein. System effectiveness parameters unique to the RPV concept will be considered.

System effectiveness is a measure of the degree to which the equipment approaches its inherent capability and achieves ease of maintenance, operation, and reliability. For purposes of this lecture, system effectiveness will be defined as shown in Figure 2. From this figure one can easily determine (using the values given in the lower right hand corner of each block) the major determinants of system effectiveness. These are indicated by the heavy dark blocks. In the remainder of the lecture the value of each block is discussed, but primary emphasis will be placed on the determinations of the probability of hit.

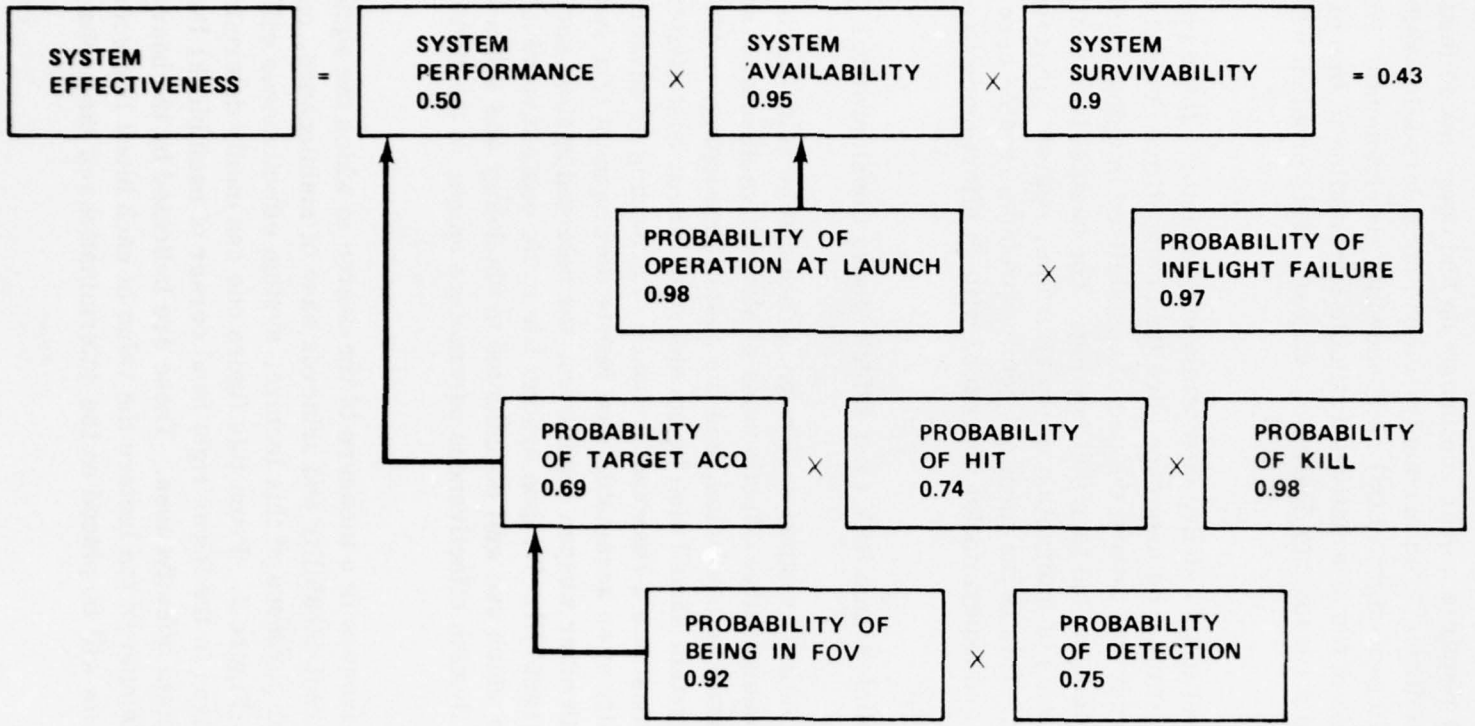

Figure 2. System effectiveness.

Design and manufacturing techniques strongly influence high availability (which often is greater than 95% for some weapon systems). The RPV availability, which includes both launch and flight reliability, should be comparable to other weapon candidates since identical technology and design techniques would be utilized in its development and manufacture.

The parameters which influence the attack RPV performance include:

1) The probability of target acquisition.

2) Probability of a hit after target acquisition.

3) Probability of kill given a hit.

Target acquisition for the attack RPV is somewhat complicated since the pilot must not only control the vehicle but also must act as an observer.

Target acquisition can be defined simply as the task of finding a known object in a complex field in a short time. The task can be defined in more detail as levels of discrimination as follows:

1) Detection, knowing an object is present.

2) Orientation, knowing the object's general shape and orientation.

3) Recognition, knowing the class or type such as truck, house, etc.

4) Identification, the object can be defined to the limit of the observer's knowledge.

For TV systems such as the one under consideration here, the following listing defines the discrimination factor, or target resolution, required for the discrimination levels previously mentioned.

Discrimination Level	Resolution Lines (TV Lines) Required	Minimum Object Dimension
Detection	2.0	+1.0 -0.5
Orientation	2.8	+0.8 -0.4
Recognition	8.0	+1.6 -0.4
Identification	12.8	+3.2 -2.8

Once a discrimination level for pilot action is established, the probability of target acquisition can be stated as the product of the probability, P_1, that a target is in the camera field-of-view (FOV) and the probability, P_2, that an adequate discrimination level is attained given a target is in the FOV. For a system such as the one under consideration here, P_1 is primarily influenced by FOV, altitude, and target location information. As a basis for discussion, assume a target array of 10 targets randomly spaced in a 2 km^2 area. Further assume that the FOV is $\pm 10°$ and the vehicle is flying at an altitude of 450 m. In this situation, the probability, P_1, that a target will enter the FOV is 0.92. Of course, P_1 will vary depending on the parameters identified earlier; however, it can be reasonably assumed that steps can be taken to assure that $P_1 \cong 0.9$. This being the case, the probability of adequate target discrimination is the most important.

A considerable amount of work has been done in an effort to establish analytical models to describe the human observer's performance in terms of target acquisition [1]. Basically, the task can be considered to consist of three distinct steps.

1) Deliberate search over a fairly well-defined area (TV screen).

2) Detection of contrast.

3) Recognition of shapes outlined by contrast contours.

For readily detectable targets (i.e., good contrast, sufficient resolution), the probability of target detection is a function of target presented area, area search rate, and scene congestion and is stated mathematically as

$$P_D = 1 - e^{(700\ at/GA)}$$

where

at = target presented area (m^2)

A = area search rate (m^2/sec)

G = scene congestion factor (possible targets per 100 × at).

Using the target array presented earlier, $P_D \simeq 0.75$ (it should be noted that this value has been verified experimentally). The corresponding value for identification would be approximately 0.65. Therefore, for a typical case the probability that the pilot will have sufficient information to attack a target will range between 0.6 and 0.7, depending on the level of discrimination required.

Another factor influencing the effectiveness is the target hit probability. If we consider rectangular targets and the mean and standard deviation of the vehicle, then the single shot hit probability can be expressed as

$$P_H = \frac{1}{2\pi}\,\sigma_Y\sigma_X \int_{-a_1}^{a_1} e^{-(x-a_2)^2/2\sigma_X^2}\,dx \cdot \int_{-b_1}^{b_1} e^{-(y-b_2)^2/2\sigma_Y^2}\,dy$$

where

σ_X, σ_Y = standard deviation in X, Y coordinates

a_1, b_1 = target dimensions in X, Y coordinates

a_2, b_2 = mean impact point relative to target center.

If we assume a typical 3×3 m target, $\sigma_X = \sigma_Y = 1.0$ m, $a_2 = b_2 = 0$, then $P_H = 0.74$.

The final factor involved in system performance is the probability of kill, P_K; i.e., the target is out of action, given a hit. For the target considered in this study and assuming modern warhead technology, P_K approaches unity. With these assumptions, the success of a single flight would range between 0.44 and 0.52; i.e.,

$$P_S = P_D \cdot P_H \cdot P_K = (0.6 \leq P_D \leq 0.7)(0.74)(1) = 0.44 \leq P_S \leq 0.52 \quad .$$

It should be noted that the previously mentioned probability of success made certain assumptions about target location information and system accuracy and points out the critical areas involved in the design of such systems. With improved system accuracy and target information, P_D could be enhanced and the probability of success will greatly improve.

The remaining effectiveness parameter unique to the RPV is survivability. There are sophisticated techniques for enhancing vehicle survivability; however, since the mini-attack RPV is to be low cost, only the simpler ones will be utilized. These include small vehicle dimensions to minimize visibility and radar cross section, muffled engine to reduce noise, and proper design to minimize infrared (IR) signature.

A qualitative summary of typical mini-attack RPV effectiveness values are presented in the following listing:

Parameter	Value
System Availability	High ~ 0.95
System Performance	Medium ~ 0.5
Probability of Detection (0.65) Probability of Hit (0.74) Probability of Kill (1.0)	
Survivability	High ~ 0.9
Operational Effectiveness	> 0.4

These parameters are utilized in war gaming studies, which may include detailed battlefield scenarios and target arrays, to determine the most cost effective weapon system when comparing the various candidates.

From this cursory consideration of system effectiveness, it is clear that system performance is of major importance and the most difficult to define. With this in mind, the remainder of this lecture will deal with the work undertaken to establish the significant parameters influencing the probability of hit. Keep in mind that the major driving force of this concept is the very low cost goal. Again, this implies a manual track and steering all the way to impact and, consequently, a strong interdependence between miss distance and vehicle flight dynamics. Therefore, the major goal of the study was to establish the feasibility and methods for analysis of a manual system. Throughout the lecture you will see references to automatic track and homing. This is included for comparison purposes and also as an alternate means for providing guidance to target impact in the event of a data link failure due to electronic countermeasures (ECM), masking, etc. Generally, the additions of an automatic tracker will increase the weapon cost to a point where desirability may be questionable.

D. Test Vehicle Design

At the initiation of this study, some preconceived ideas (not all necessarily sound) governed the selection of the design and the direction of the experiments. The first idea was that the most efficient airframe would

resemble a conventional airplane and utilize a roll to turn control scheme. The second was that the acquisition requirements could be best met by a relatively slow (≤ 70 m/sec) vehicle. The size then would be compatible with the payload and structural requirements. The third idea was that the cost, survivability, and troop handling goals all required as small and lightweight airframe as possible.

The first step was to generate a realistic test vehicle with these preconceived ideas.

The preliminary design was biased toward the preconceived ideas and by the need to use only existing components to speed the program and reduce cost. Therefore, much of the preliminary design process resulted from an intuitive exercise. Therefore, the approach in the presentation is similar.

Figure 3 is a schematic view of the initial airframe. This configuration was chosen primarily on the following points:

1) The pusher allowed complete freedom in configuring the payload package. Since the vehicle would use a two-cycle reciprocating engine, the pusher also allowed easy solution to the exhaust pollution of the payload.

2) The single boom lended itself to the catapult launch planned for the program.

3) The low number of vehicles (3) constructed did not make reinforced plastic molding economical. Therefore, this configuration allowed easy construction using conventional light aircraft techniques.

Weight was a problem because of limited power available. A survey of available power plants indicated no good power/weight ratio engines were available in the 10cc and 80cc range. We were not interested in an engine development; therefore, the decision was to use the available 10cc engines. This limited the available horsepower to approximately 1.5. Weight had to be kept to a minimum to achieve a reasonable power to weight ratio.

Detailed weights of the resulting vehicle are given in Figure 4. All aerodynamic surfaces were constructed with a foam core (2.43 kg/m^3) with a balsa skin covered with a 0.0015 in. mylar sheet. The fuselage is a three piece wood and plywood structure. The landing skid also serves as the catapult drive.

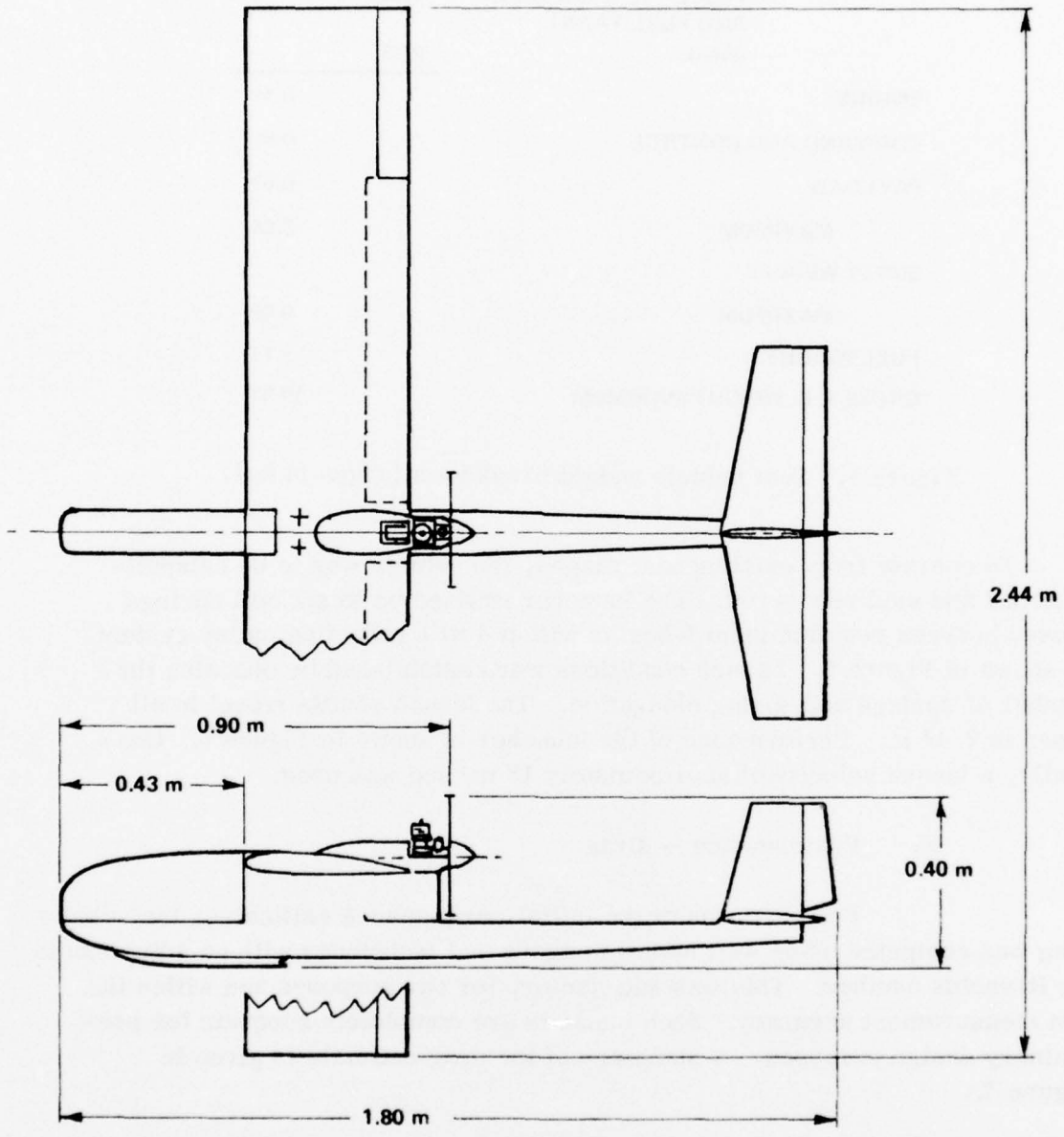

Figure 3. Test vehicle general arrangement for Phase I.

AIRFRAME	– TAIL	0.37	
	– FUSELAGE (FAIL SAFE AND FUEL TANK)	2.44	
	– WING	2.33	
ENGINE			5.14
COMMAND AND CONTROL			0.51
PAYLOAD			0.63
MAXIMUM			3.54
EMPTY WEIGHT			
MAXIMUM			9.82
FUEL WEIGHT			1.11
GROSS T. O. WEIGHT MAXIMUM			10.93

Figure 4. Test vehicle weight breakdown (given in kg).

To operate from existing test ranges, the vehicle was to be catapult-launched and skid recovered. The launcher utilized up to six coil springs housed between two aluminum I-beams with a 4 to 1 reduction pulley system as shown in Figure 5. Launch conditions were established by choosing the number of springs and spring elongation. The launch shuttle travel in all cases is 2.44 m. Performance of the launcher is shown in Figure 6. Generally, a launch velocity of approximately 18 m/sec was used.

E. Performance – Drag

For purposes of the initial performance estimates, the vehicle drag was computed using well known methods and techniques with no adjustments for Reynolds number. This was satisfactory for our purposes and within the test measurement accuracy. Such methods are completely adequate for preliminary design purposes. A summary of the drag estimate is given in Figure 7.

The drag as a function of velocity and weight using the values of Figure 7 is shown in Figure 8.

F. Performance – Thrust Available

The largest source of inaccuracy in predicting available thrust for this class of engine is the knowledge of the power versus rpm, since it varies so much from engine to engine and depending on fuel mixture. For this study the only available performance was that shown in Figure 9.

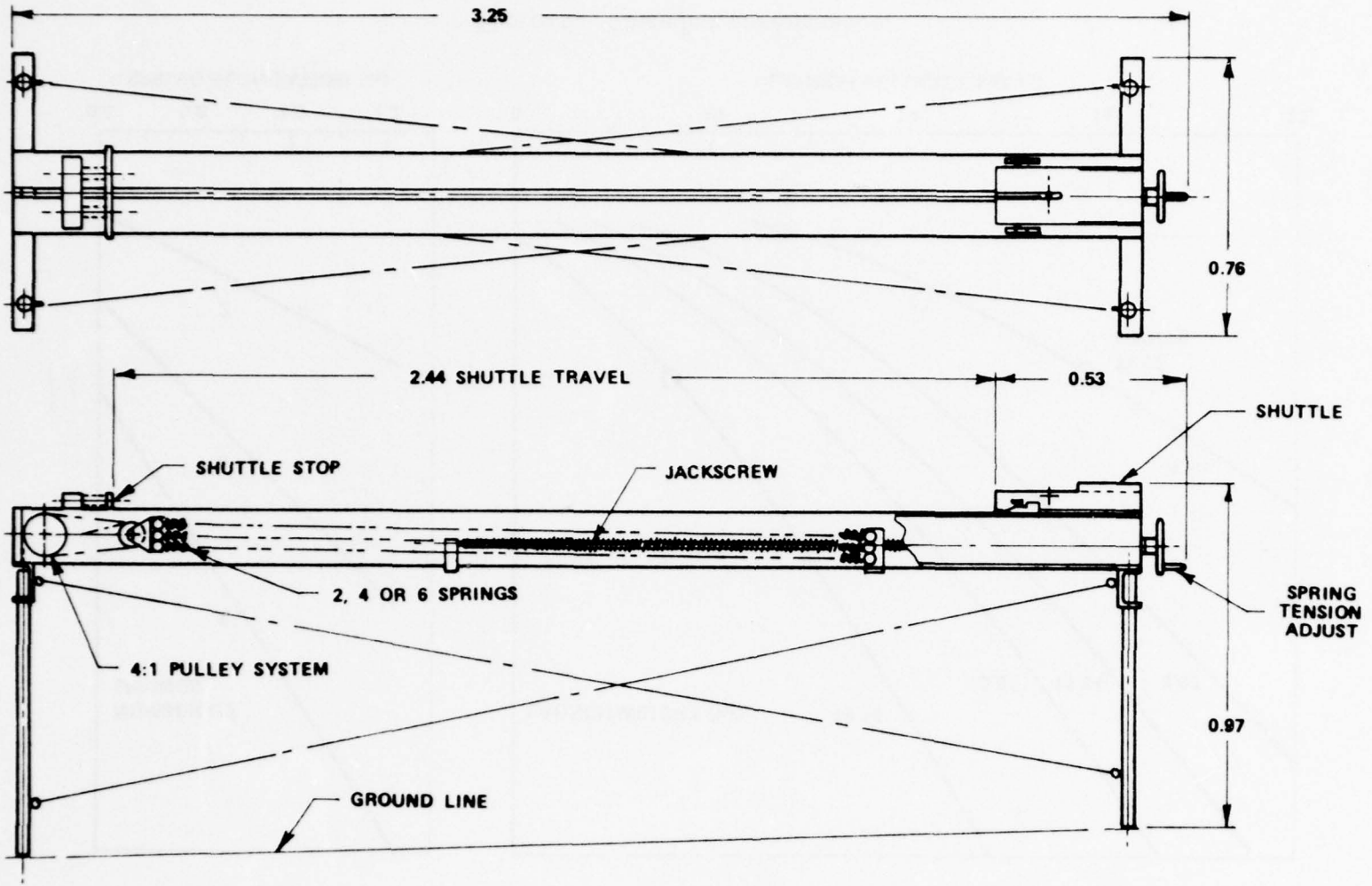

Figure 5. Launcher layout.

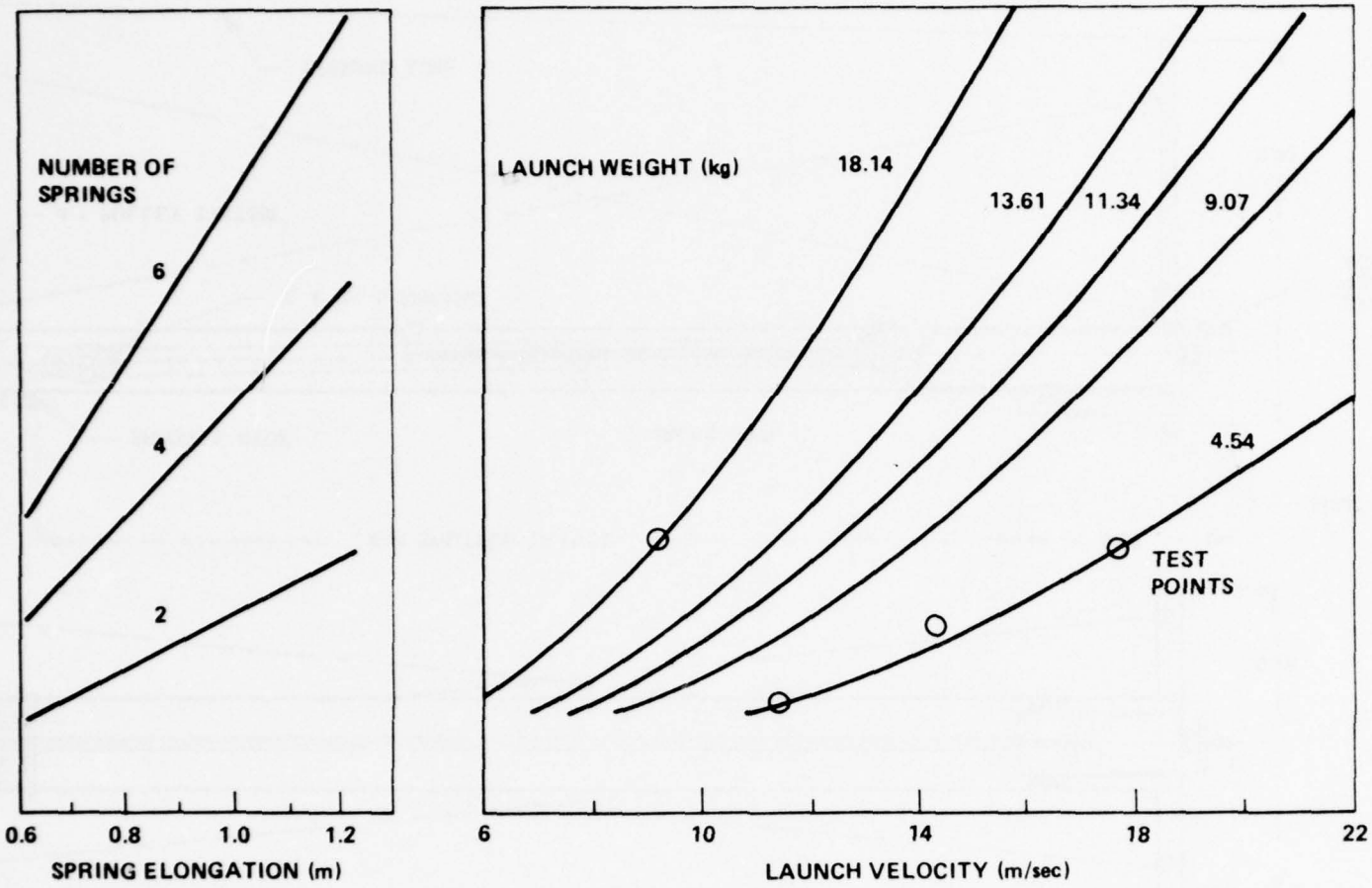

Figure 6. Launcher performance.

1. PARASITIC

FUSELAGE	– SKIN FRICTION (REFERENCE 2)	0.0055
	– PROTURBENCES (ENGINES, OPTICS, ETC.)	0.0016
	– PRESSURE DRAG (REFERENCE 2)	0.0033
TAIL	– ZERO LEFT PROFILE DRAG	0.0016
	C_{CP} =	0.0120

2. TOTAL DRAG $C_D = C_{CO} + C_{DL} + C_{DP}$

C_{DO} – SECTION DRAG COEFFICIENT FOR NACA 23015

f (C_L) (REFERENCE 3)

$$C_{DL} = \frac{1+\delta}{\pi\, AR}\, C_L^2 = 0.0545\, C_L^2 \text{ (REFERENCE 4)}$$

Figure 7. Drag estimation.

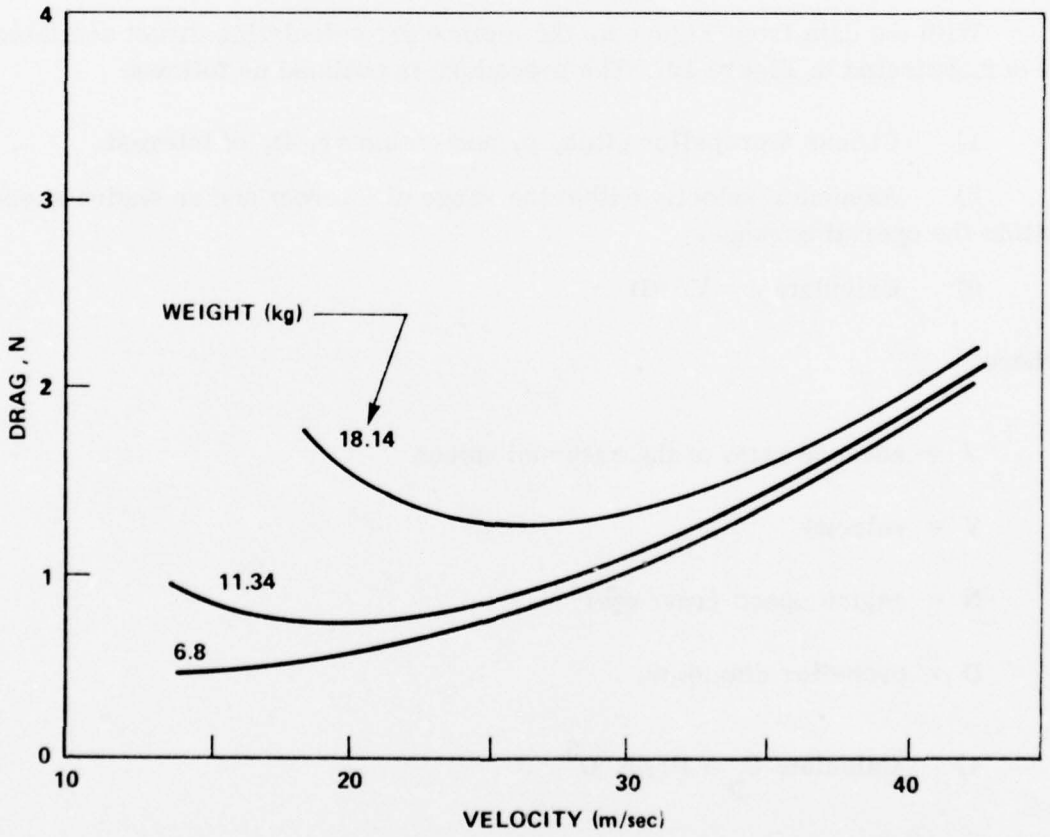

Figure 8. Vehicle drag.

RPM	HORSEPOWER (550 ft–lbf/sec)
10,5000	1.00
11,000	1.02
11,500	1.06
12,000	1.08
12,500	1.10
13,000	1.12
13,500	1.13
14,000	1.14
14,500	1.14
15,000	1.13

Figure 9. Engine horsepower versus rpm.

With the data from Figure 9, the method for calculating thrust available is demonstrated in Figure 10. The procedure is outlined as follows:

1) Choose a propeller pitch, p, and diameter, D, of interest.

2) Assume a velocity within the range of interest and an engine speed within the operating range.

3) Calculate $J = V/ND$

where

J = advance ratio of the assumed values

V = velocity

N = engine speed (rev/ sec)

D = propeller diameter.

4) Calculate $C_p = P/\rho N^3 D^5$

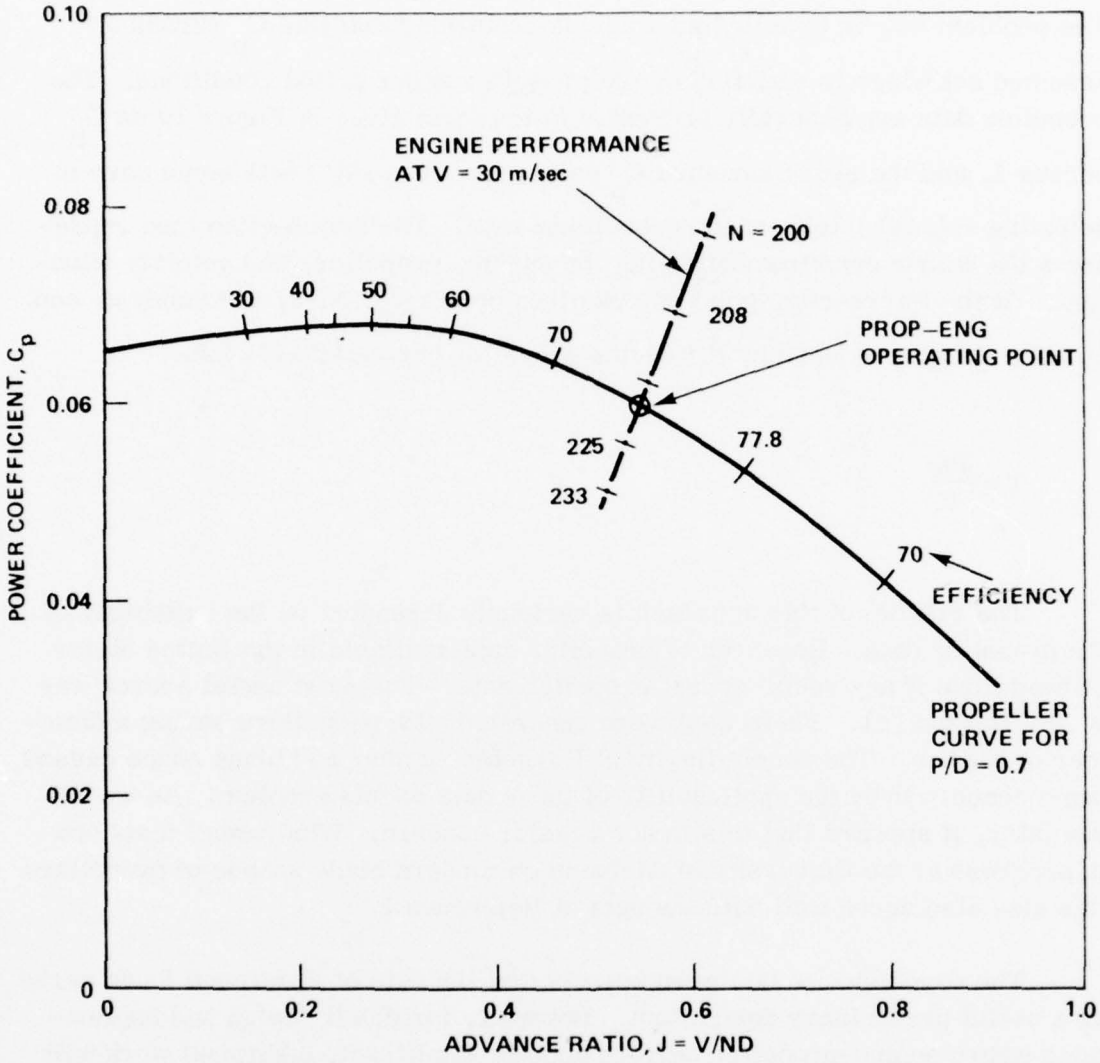

Figure 10. Propeller-engine operating point.

where

P = engine shaft horsepower (from Figure 9)

ρ = atmospheric density.

5) Repeat steps 1 through 4 for other values of V, P, and N.

The problem now is to establish a unique condition from this C_p versus J assumed set which is satisfied by the propeller under actual conditions. The propeller data are generally presented in the form given in Figure 10 as C_p versus J, and the set of assumed C_p versus J values will (with some care in selecting values) intersect the propeller curve. The intersection then represents the unique condition satisfying the engine, propeller, and velocity situation. At the intersection point one can then obtain C_p, N, J, efficiency n, and P. The thrust produced by the engine propeller combination is then

$$T = \frac{P\eta}{V} \quad .$$

The validity of this approach is obviously dependent on the suitability of the propeller data. Research of propeller data available in the United States showed little if any useful recent propeller data. The most useful source was W. E. Durand [5]. These data were generated with propellers having a diameter of 0.61 m. The nonsimilarity of Reynolds number and blade shape caused some concern over the applicability of these data to this problem. As we will see later, it appears that this is not a major concern. Wind tunnel tests now in progress at the University of Alabama on modern blade shapes of propellers this size also agree well with the data of Reference 5.

The conclusion to be drawn here is that the data of Reference 5 can serve as a useful preliminary design tool. However, for detail design and applications where engine-propeller performance is significant, additional work will be required to fit a specific application.

If one desires to find an optimum propeller for a given engine to maximize thrust at a given velocity, the so-called speed power coefficient is of use. The speed power coefficient, C_s, is defined as

$$C_s = V \sqrt[5]{\frac{\rho}{PN^2\ 550}} = \frac{J}{\sqrt[5]{C_p}} \quad .$$

Figure 11 shows the propeller data from Reference 5 at various P/D's with C_s superimposed. Now if one determines N at maximum engine power, P, then C_s can be computed. From Figure 11 one can determine the J and P/D which maximizes the efficiency, n. With J and P/D the propeller size and pitch may be determined.

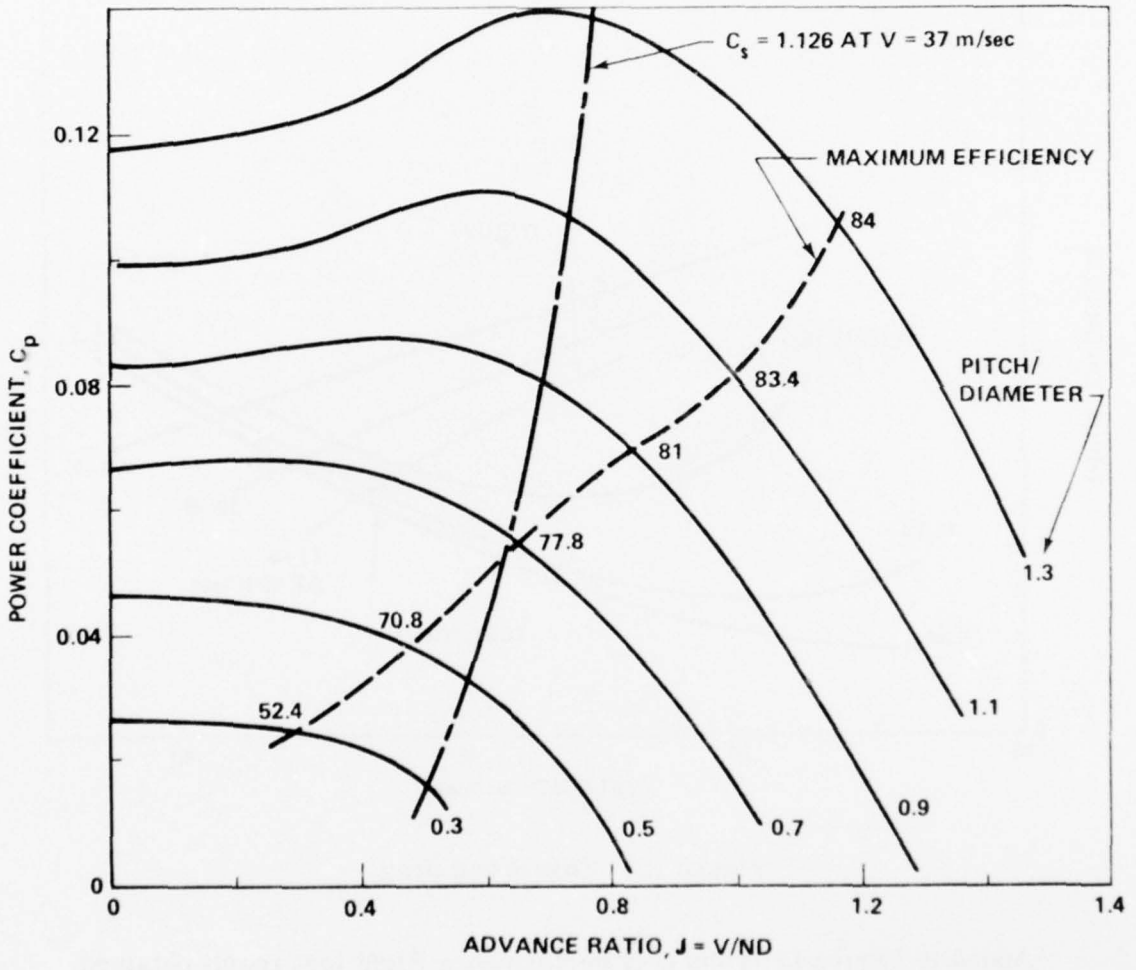

Figure 11. Speed power coefficient.

Using the previously mentioned technique, a specific propeller-engine combination performance may be established in terms of thrust versus velocity. Adding this to the data on Figure 8, the result is Figure 12 from which the expected aircraft performance may be determined.

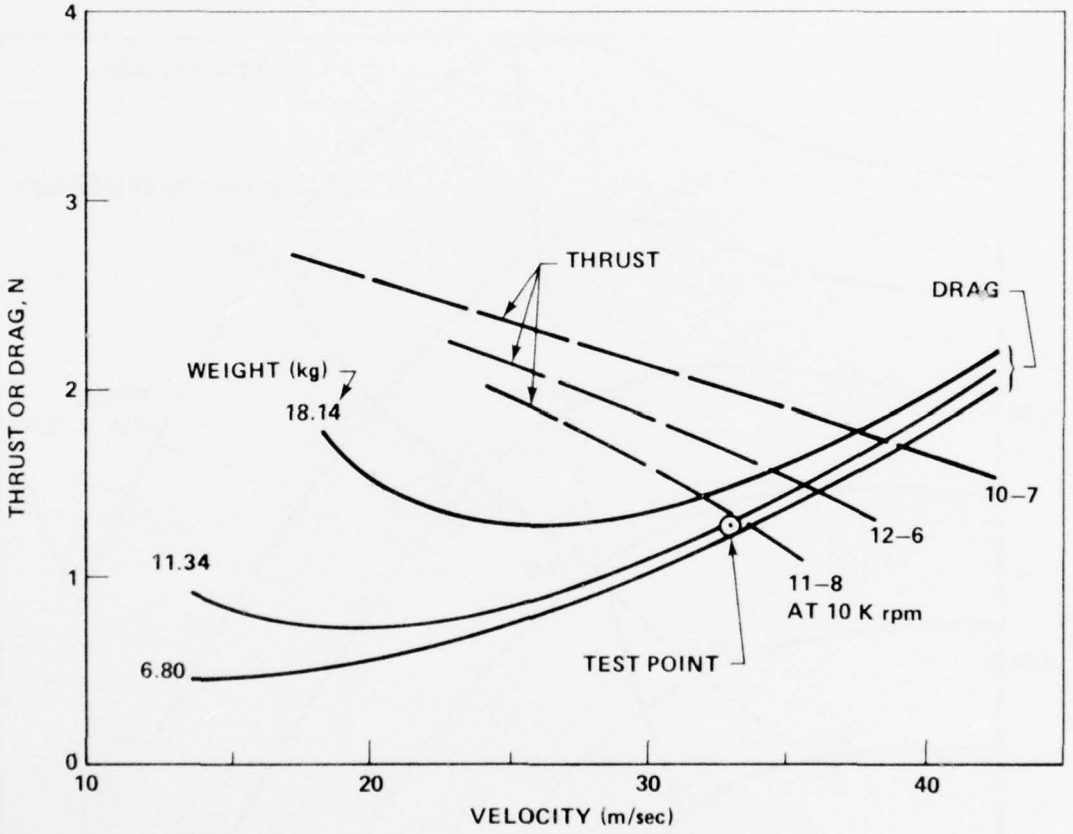

Figure 12. Thrust and drag.

Added to Figure 12 is the only performance flight test result obtained. This shows close agreement and will be useful for preliminary design. Mechanization of the previously mentioned method on small computers has served as a useful tool for preliminary design of other RPV and drone aircraft.

G. Control and Telemetry Links

For the test vehicle the major item governing the control and telemetry links was the availability of components. Since ECM was not a problem, it was possible to make use of commercially available hardware.

The ground control station consisted of three major pieces of equipment. The first, the pilot' s control box, was developed from a Kraft R/C system using either two — two-axis sticks or a single three-axis stick with auxiliary controls. Outputs from the control box were used to pulse width modulate an RF transmitter unit. All control data were transmitted to the aircraft using seven proportional channels. The second piece of equipment is the video display. This was provided by an FM-FM down link telemetry system. The ground portion of this consisted of a 4-ft parabolic receiving antenna, which in our case was manually tracked using the receiver signal strength indicator on a conic CVR FM-3 receiver. This was followed by appropriate discriminators to provide a video display and flight data recording. The third major ground station item was the secondary pilot control box which was identical to the pilot' s and always had override capability. This was solely provided for safety purposes in the event of pilot control or video data link problems.

The airborne control system consisted of the command receiver, decoder and electromechanical servo, TV camera, and telemetry down link transmitter. The receiver and decoder provided the seven control channels. Four of these channels were used for pitch, roll, yaw, and throttle control; the remaining three were used for FOV control, autopilot, and any desired auxiliary function.

The complete control system is shown in Figure 13.

II. SYSTEM SIMULATION

A. General

The primary objective of the mini-RPV simulation developed at the US Army Missile Research and Development Command (MIRADCOM) Redstone Arsenal, Alabama was to provide a tool for the determination of the feasibility of an attack RPV. Emphasis was placed on the terminal trajectory and on finding solutions to problems that were identified in earlier experimental work. The effects on system performance, as measured by target miss

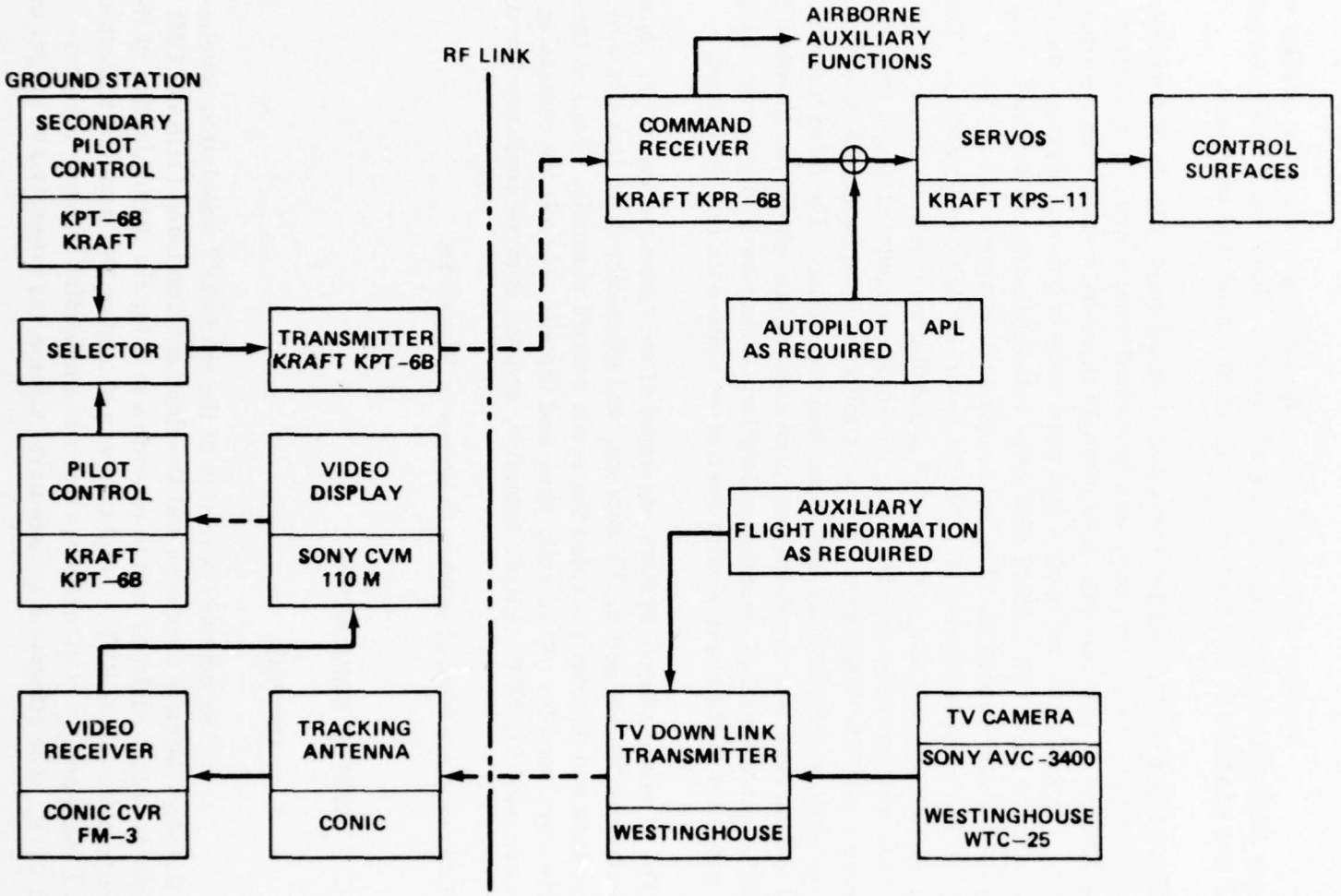

Figure 13. RPV control diagram.

distance, resulting from variations in certain system parameters were investigated. In addition, the pilot's performance was determined in terms of adaptation to the terminal trajectory task. Finally, the simulation was used to investigate terminal guidance schemes other than those employing a human controller.

The baseline physical system modeled by the simulation is a small, single boom pusher aircraft shown in Figure 3. This aircraft was constructed for a program to demonstrate the ability to manually fly and perform an attack via TV link. Flight test with the baseline system indicated difficulty for the operator to perform successful intercept. As a result, considerable simulation effort was directed toward alternate designs which would provide improved man-aircraft performance. Therefore, the simulation effort consisted of an evaluation of the baseline configuration, designated C0, and variations about it as shown in Figure 14. These airframe variations resulted from a desire to roll stabilize the target image presented to the pilot. Table 1 provides a summary of significant physical parameters for the configurations simulated.

B. Equations of Motion

The classical Euler equations of motion, the derivation of which are found in the literature, were used in the simulation. These equations are derived with respect to a set of axes fixed to the aircraft body and rolling with it (Figure 15). The equations in vector form are

$$F = m \frac{dv}{dt} + m\omega \times v \tag{1}$$

$$H = \frac{dh}{dt} + \omega \times h \tag{2}$$

where F is the resultant external force vector and H is the resultant external moment vector about the center of gravity. These equations have the scalar components

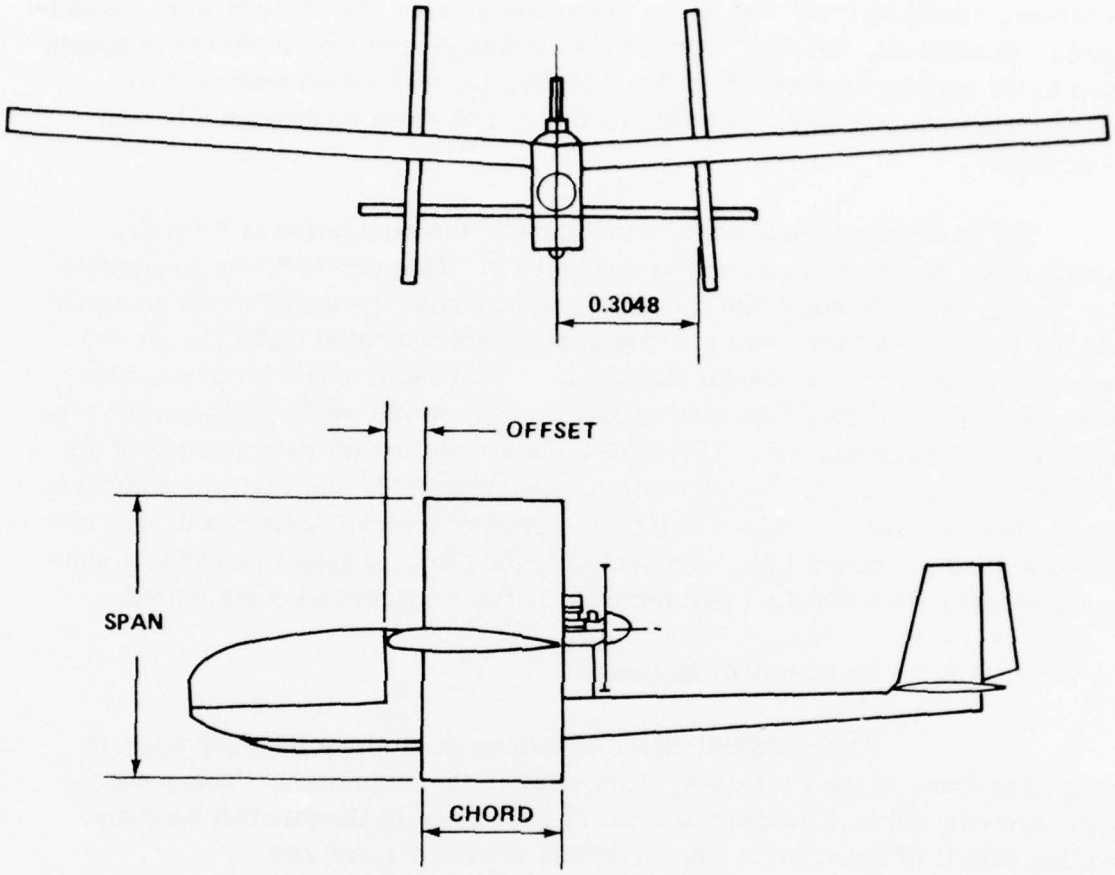

	CONFIGURATION			
C_{Y_β} (per rad β)	1.421	1.043	0.602	1.043
C_{N_β} (per rad β)	−0.427	−0.304	−0.366	−0.304
CHORD (m)	0.3048	0.381	0.381	
SPAN (m)	0.6096	0.4572	−0.3048	0.4572
REARWARD OFFSET FROM WING LEADING EDGE (cm)	7.62	0	0	0
FRACTION OF SPAN BELOW MAIN WING CHORD LINE	0.5	0.5	0.5	0.33

Figure 14. Vertical wing configurations.

TABLE 1. VEHICLE CHARACTERISTICS

Configuration C0		
Type	Small winged aircraft	
Power	Webra model a/c engine, 2-cycle reciprocating; Displacement 10cc; Maximum horsepower 1.14 at 14,000 rpm	
Size	Span	2.4384 m
	Wing area	0.929 m^2
	Length	1.8034 m
	Payload volume	0.0084 m^3
Weight	Total test vehicle (10.1-lb payload) See Figure 4	10.206 kg
Flight control	Kraft 6-channel proportional	72.08 MHz

Configurations	C1	C2	C3	C4
Weight: Vertical wing gross weight (kg)	1.36	1.28	0.63	1.28

$$\left.\begin{aligned} F_x &= m(\dot{u} + qw - rv) \\ F_y &= m(\dot{v} + ru - pw) \\ F_z &= m(\dot{w} + pv - qu) \end{aligned}\right\} \quad \text{Force} \qquad (3)$$

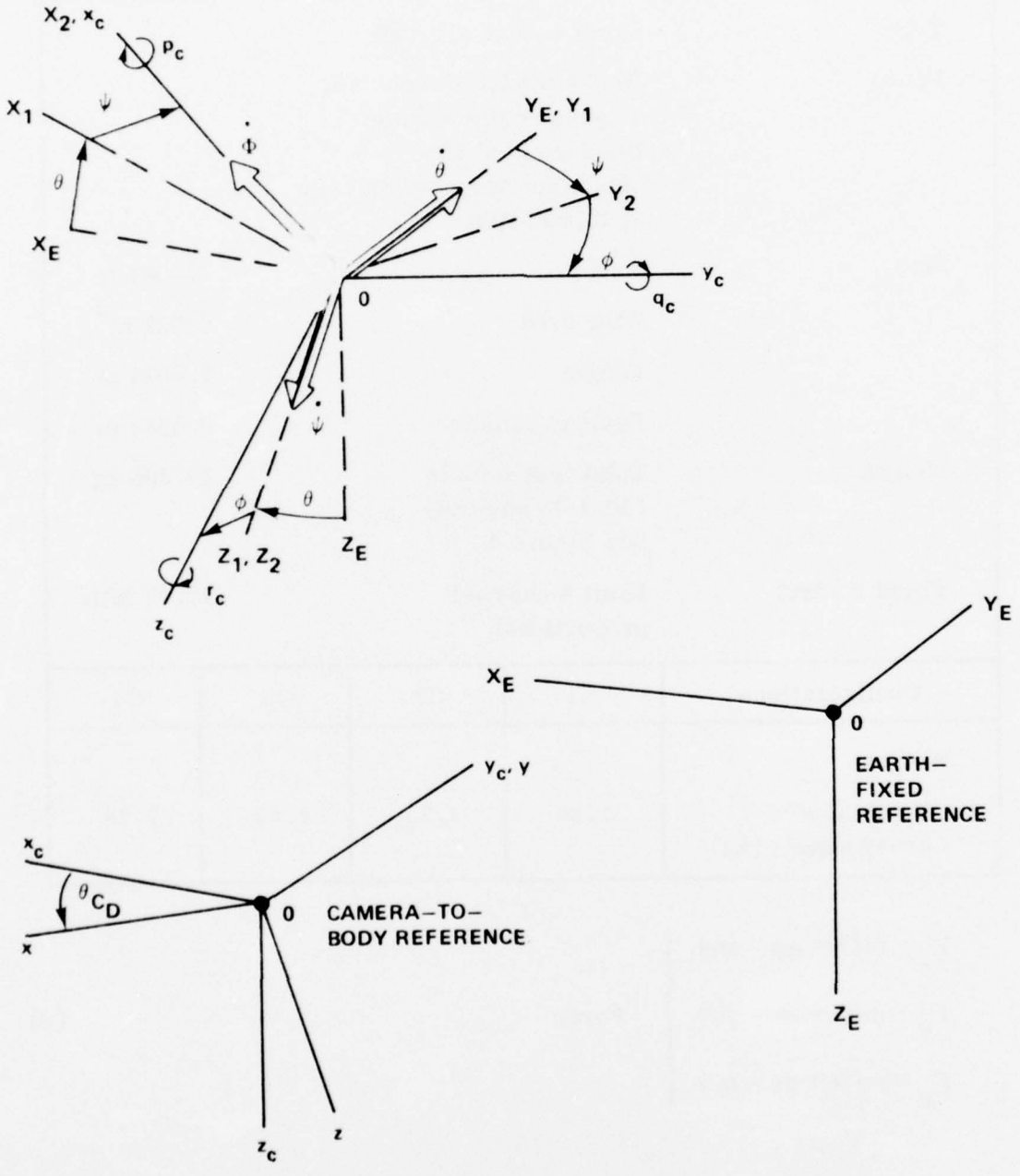

Figure 15. Coordinate systems.

$$\left.\begin{aligned} L &= \dot{p}I_x + qr(I_y - I_z) \\ M &= \dot{q}I_y + pr(I_x - I_z) \\ N &= \dot{r}I_z + pq(I_y - I_x) \end{aligned}\right\} \quad \text{Moment} \tag{4}$$

where

$$F_x = T - D - mg \sin \theta$$

$$F_y = -QS\left(C_{y_\beta}\beta + C_{y_{\delta_r}}\delta_r\right) + mg \cos \theta \sin \phi$$

$$F_z = -QS\left(C_{L_{\alpha_w}}\alpha_w + C_{L_{\delta_e}}\delta_e\right) + mg \cos \theta \cos \phi \tag{5}$$

$$L = QSb\left[C_{\ell_{\delta_a}}\delta_a + \left(C_{\ell_r} - C_{\ell_p}\right)\frac{pb}{2V} - C_{\ell_\beta}\beta + C_{\ell_{\delta_r}}\delta_r\right]$$

$$M = QSc\left[C_{M_0} - C_{M_{\alpha_w}}\alpha_w - C_{M_q}\frac{qc}{2V} - C_{M_{\delta_e}}\delta_e\right]$$

$$N = QSb\left[C_{N_\beta}\beta - \left(C_{N_r}r + C_{N_p}|\alpha_w|p\right)\frac{b}{2V} + C_{N_{\delta_r}}\delta_r\right] \tag{6}$$

and

$$T = \left(-2.7 \times 10^{-6}\right) \text{ rpm } V + \left(7.2 \times 10^{-4}\right) \text{ rpm} \tag{7}$$

$$D = QS\, C_{A0} \tag{8}$$

$$C_{A0} = 0.019 + 1.173\, \alpha_w^2 \tag{9}$$

$$Q = 1/2\,\rho V^2 \tag{10}$$

$$\alpha_w = \alpha + 0.0524 \tag{11}$$

$$\alpha = \frac{w}{u} \tag{12}$$

$$\beta = \frac{v}{u} \quad . \tag{13}$$

Since the aircraft is designed as a platform for an unstabilized TV camera, an electrostatic autopilot [6] is employed to provide pitch and roll stability. The electrostatic autopilot, which consists of radioactive sensors placed on the wing tips and nose of the aircraft and connected to two differential voltmeters, depends upon the fact that the atmosphere contains equipotential electrical fields that are a function of altitude. It is then possible, with this arrangement, to detect the altitude difference between the wing tips (roll detection) and between the nose and wing (pitch detection). This information is used to deflect the ailerons and elevator such as to counteract the roll and pitch motion of the aircraft. The autopilot is represented mathematically by

$$\begin{aligned} \Delta\delta_a &= -K_r f_r(Z) \\ \Delta\delta_e &= -K_p f_p(Z) \end{aligned} \tag{14}$$

where K_r and K_p are the autopilot gain factors and $f_r(Z)$ and $f_p(Z)$ are the sensor positions as a function of altitude Z. The equations for the control surfaces deflections are

$$\delta_a = K_{\delta_a} \lambda_a + \Delta\delta_a$$

$$\delta_e = K_{\delta_e} \lambda_e + \Delta\delta_c \qquad (15)$$

$$\delta_r = K_{\delta_r} \lambda_r$$

where K_{δ_a}, K_{δ_c}, and K_{δ_r} are the respective fixed stick control gains and λ_a, λ_e, and λ_r are the stick angular positions.

The forces and moments in Equations (3) through (9) are the external actions upon the vehicle. They are of two kinds, gravitational and aerodynamic, and are determined by the variables (p, q, r) (δ_e, δ_a, δ_r), (u, v, w), and (θ, ψ, ϕ). The control forces, however, are internal forces determined by the commands of a human or autopilot.

To determine the aircraft position and orientation, we define a fixed frame of reference $0X_E Y_E Z_E$ as shown in Figure 15. The orientation of the aircraft is determined by three consecutive ordered rotations. Assuming the aircraft is initially aligned with $0X_E Y_E Z_E$, its orientation is found by

1) θ rotation — providing the elevation.

2) ψ rotation — providing the azimuth.

3) ϕ rotation — providing the bank angle.

To calculate the aircraft flight path, the velocity components in the 0XYZ coordinate system are resolved into the $0X_E Y_E Z_E$ system and integrated. The transformations relating these two coordinate systems are

1) Earth to body —

$$[c] = [\phi]\ [\psi]\ [\theta] \qquad (16)$$

where

$$[\theta] = \begin{pmatrix} \cos\theta & 0 & -\sin\theta \\ 0 & 1 & 0 \\ \sin\theta & 0 & \cos\theta \end{pmatrix} \tag{17}$$

$$[\psi] = \begin{pmatrix} \cos\psi & \sin\psi & 0 \\ -\sin\psi & \cos\psi & 0 \\ 0 & 0 & 1 \end{pmatrix} \tag{18}$$

$$[\phi] = \begin{pmatrix} 1 & 0 & 0 \\ 0 & \cos\phi & \sin\phi \\ 0 & -\sin\phi & \cos\phi \end{pmatrix} . \tag{19}$$

2) Body to earth —

$$[c]^{-1} \quad [\theta]^{-1} [\psi]^{-1} [\phi]^{-1} \tag{20}$$

where

$$[\theta]^{-1} = \begin{pmatrix} \cos\theta & 0 & \sin\theta \\ 0 & 1 & 0 \\ -\sin\theta & 0 & \cos\theta \end{pmatrix} \tag{21}$$

$$[\psi]^{-1} = \begin{pmatrix} \cos\psi & -\sin\psi & 0 \\ \sin\psi & \cos\psi & 0 \\ 0 & 0 & 1 \end{pmatrix} \tag{22}$$

$$[\phi]^{-1} = \begin{pmatrix} 1 & 0 & 0 \\ 0 & \cos\phi & -\sin\phi \\ 0 & \sin\phi & \cos\phi \end{pmatrix} \quad . \tag{23}$$

The angular orientation (θ, ψ, ϕ) can be determined in terms of the aircraft angular velocity components (p, q, r) by projecting the total angular velocity ω onto 0XYZ, recalling that $\omega = ip + jp + kr$. The relations obtained are

$$\begin{aligned} \dot{\phi} &= p - \dot{\theta} \sin\psi \\ \dot{\theta} &= (q \cos\phi - r \sin\phi) \sec\psi \\ \dot{\psi} &= q \sin\phi + r \cos\phi \quad . \end{aligned} \tag{24}$$

Integration then gives

$$\begin{aligned} \phi &= \int \dot{\phi} + \phi_0 \\ \theta &= \int \dot{\theta} + \theta_0 \\ \psi &= \int \dot{\psi} + \psi_0 \quad . \end{aligned} \tag{25}$$

To find the vehicle position relative to the $0X_E\ Y_E\ Z_E$ coordinate system, we have the acceleration terms

$$\begin{pmatrix} \ddot{X}_E \\ \ddot{Y}_E \\ \ddot{Z}_E \end{pmatrix} = [c]^{-1} \begin{pmatrix} u \\ v \\ w \end{pmatrix} \tag{26}$$

which are then integrated to find position.

The primary output desired from the simulation is the aircraft impact point in relation to a known target. If the target position is defined in the earth-fixed system $0X_E\ Y_E\ Z_E$ as (X_T, Y_T, Z_T) and the aircraft position as (X_M, Y_M, Z_M), then the aircraft-target separation is simply

$$\begin{aligned} \Delta X &= X_T - X_M \\ \Delta Y &= Y_T - Y_M \\ \Delta Z &= Z_T - Z_M \end{aligned} \tag{27}$$

C. Aircraft Aerodynamic Coefficients

To set up the computer simulation, it was necessary to compute the aerodynamic coefficients called for in the flight equations. These coefficients were computed as a first approximation to be subsequently refined by flight data; hence, classical aircraft theory was used. The effects of Mach number and low Reynolds number were ignored. This is justified by the fact that almost all of the data taken involved a constant velocity of 30 m/sec. The Reynolds number at this velocity is 8×10^5, and effects of Reynolds number are not significant at this value. The primary reference for the computation of the aerodynamic coefficients was Perkins and Hage [7]. Table 2 provides a summary of the vehicle parameters used to generate the aerodynamic coefficients, and Table 3 presents the resulting coefficients.

The vertical stabilizer wings have three main effects on the aircraft aerodynamics: (1) increased side force coefficient C_{y_β}, (2) an increase in aircraft drag (primarily induced), and (3) a change in the yaw moment coefficient C_{M_β}. Configurations C1, C2, C3, and C4 are conceptually the same but with differing vertical wing areas and placement.

The assumptions made and the methods used in generating the necessary aerodynamic coefficients was greatly influenced by the type of investigations to be conducted. The primary attempt in the simulation was to reasonably simulate the flight characteristics of a mini-RPV in an attack role, and the

TABLE 2. INPUT DATA FOR AERODYNAMIC COEFFICIENTS

Parameter		Wing
E	Jones edge-velocity factor	1.03
a_ω	Three-dimensional lift curve slope	0.081/deg α
AR	Aspect ratio	6.4
c	Chord	0.381 m
b	Span	2.4384 m
S	Wing area	0.929 m^2
x_{AC}	Wing aerodynamic center	24% c from LE
τ_a	Aileron effectiveness factor	0.35
Parameter		Vertical Tail
S_f	Area	0.0577 m^2
a_v	Lift curve slope	0.045/deg β
τ_v	Rudder effectiveness factor	0.49
ℓ_v	Distance from cg to tail aero center	1.079 m
n_v	Velocity differential V_f/V_w	1.6
z_f	Aero center above vertical cg	0.067 m
Parameter		Horizontal Tail
S_t	Area	0.1605 m^2
a_t	Lift curve slope	0.075
τ_t	Elevator effectiveness factor	0.49
n_t	Velocity differential V_t/V_w	0.95
ℓ_t	Wing aero center to tail aero center	1.015 m
$\overline{V}$	$S_t/S_w \ell_t/c$	0.46

TABLE 2. (Concluded)

Parameter		Fuselage
x_{cg}	Center of gravity	38% c from LE
K_f	Stability coefficient	0.01
W_f	Maximum width	0.1059 m
ℓ_f	Length	1.8034 m
K_β	Directional stability coefficient	0.1
h_1	Height at $1/2\ \ell_f$	0.2433 m
h_2	Height at $3/4\ \ell_f$	0.06 m
w_1	Width at $1/2\ \ell_f$	0.1059 m
w_2	Width at $3/4\ \ell_f$	0.074 m
S_s	Side area	0.282 m^2

Vertical Wing Data for Configurations C1, C2, C3, and C4

Parameter	C1	C2	C3	C4
Chord (m)	0.3048	0.381	0.381	0.381
Span (m)	0.6096	0.4572	0.3048	0.4572
Offset from wing LE (cm)	7.62	0	0	0
Fraction of span below wing	0.5	0.5	0.5	0.33

TABLE 3. AERODYNAMIC COEFFICIENTS

Parameter	Value
C_{N_α}	4.64/ rad α
$C_{\ell_{\delta_e}}$	0.356/ rad δ_e
$C_{\ell_{\delta_r}}$	0.0034/ rad δ_r
C_{ℓ_p}	0.51/ rad
C_{ℓ_β}	0.0478/ rad β
$C_{y_{\delta_r}}$	0.125/ rad δ_r
C_{y_β} : (C0) *See Figure 14*	0.159/ rad β 1.421/ rad β 1.043/ rad β 0.602/ rad β 1.043/ rad β
C_{M_0}	0.013
C_{M_α}	0.332/ rad α
C_{M_q}	1.653/ rad
$C_{M_{\delta_e}}$	0.917/ rad δ_e
C_{n_β} (C0) See Figure 14	0.199/ rad β
C_{n_r}	0.082/ rad
C_{n_p}	0.58/ rad α
$C_{n_{\delta_r}}$	0.055/ rad δ_r

TABLE 3. (Concluded)

Parameter	Value
C_D: C0	$0.019 + 1.173\alpha^2$
C1	$0.0214 + 1.173\alpha^2 + 0.79\beta^2$
C2	$0.0213 + 1.173\alpha^2 + 0.62\beta^2$
C3	$0.0205 + 1.173\alpha^2 + 0.33\beta^2$
C4	$0.02 + 1.173\alpha^2 + 0.62\beta^2$

results shown later should be viewed in a comparative manner. Because of the foregoing consideration, it is believed that the aerodynamic data used in the simulation is quite adequate. Implementation of a particular design would require a more thorough aerodynamic analysis.

D. The Electrooptical Simulation System (EOSS)

The EOSS, depicted schematically in Figure 16 and shown pictorally in Figure 17, provides realistic and precisely controlled environments for the nondestructive simulation of a wide variety of ultraviolet, visable, and near IR sensor systems. The capabilities of the EOSS provide for six degrees of freedom (6DOF), viz: three degrees of rotational motion and three degrees of translational motion. The three degrees of rotation are provided by a three-axis, gimbaled flight table where the sensor is mounted in the inner (roll) gimbaled housing. The flight table provides for all missile body angular displacements, body rates, and accelerations required for open-loop or closed-loop simulation. The three degrees of translational motion are provided by three transport subsystems. The lateral transport moves the flight table in a horizontal beam. A vertical beam assembly operates through an end box/ rack and rail inside the vertical column housing structure. This translation provides all vertical or altitude displacements, rates, and accelerations. The longitudinal transport system moves the terrain/ target model through a carriage-interfaced rack and rail assembly toward the flight table. This longitudinal travel provides range closure displacements, rates, and accelerations. The longitudinal subsystem transports the three-dimensional terrain/ target model. Three-dimensional targets are simulated on the terrain model which features a variety of topography and man-made complexes at 600:1 and 300:1 scales with the capability to add fixed and moving targets at any scale.

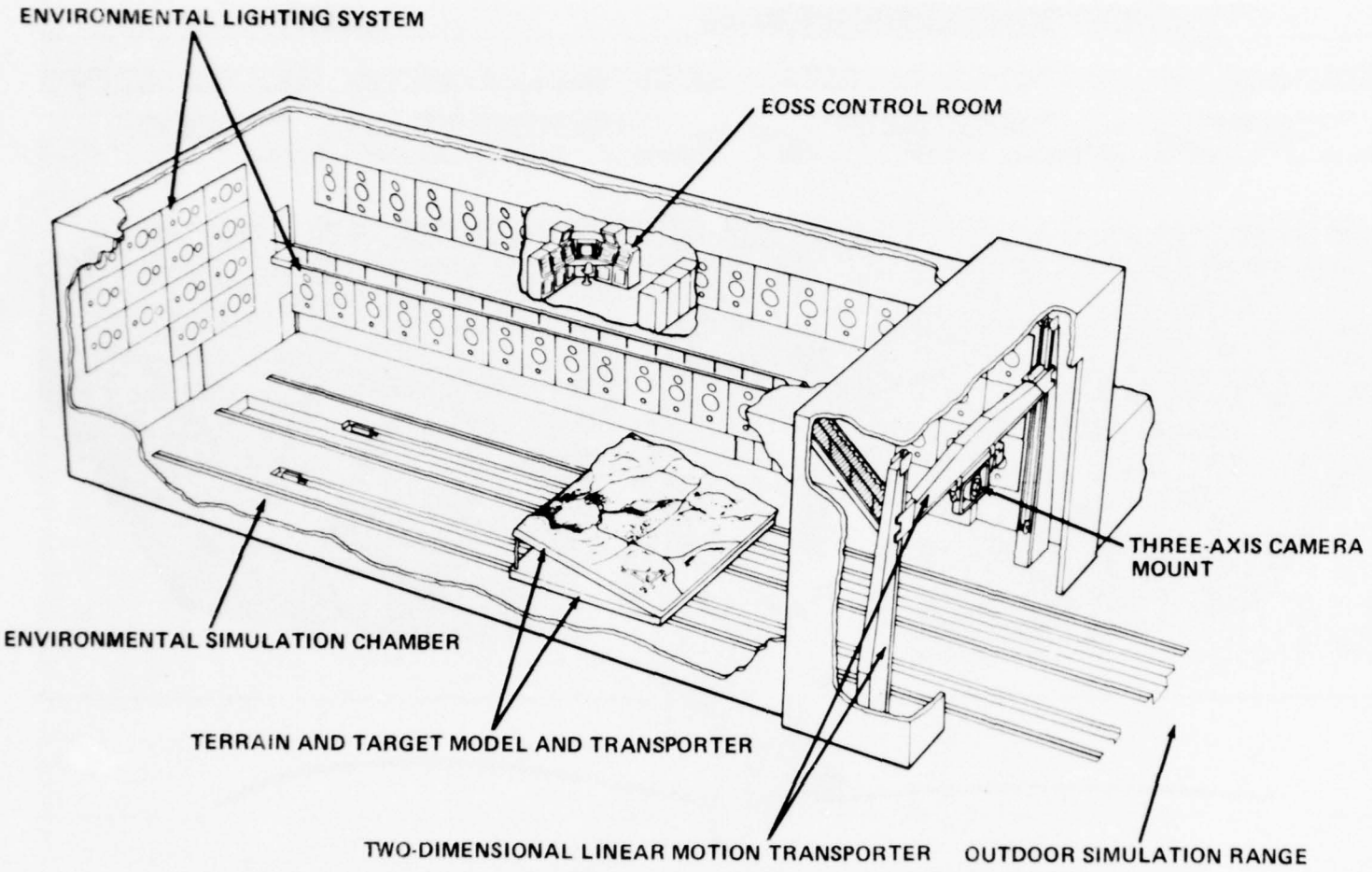

Figure 16. Electrooptical simulation system.

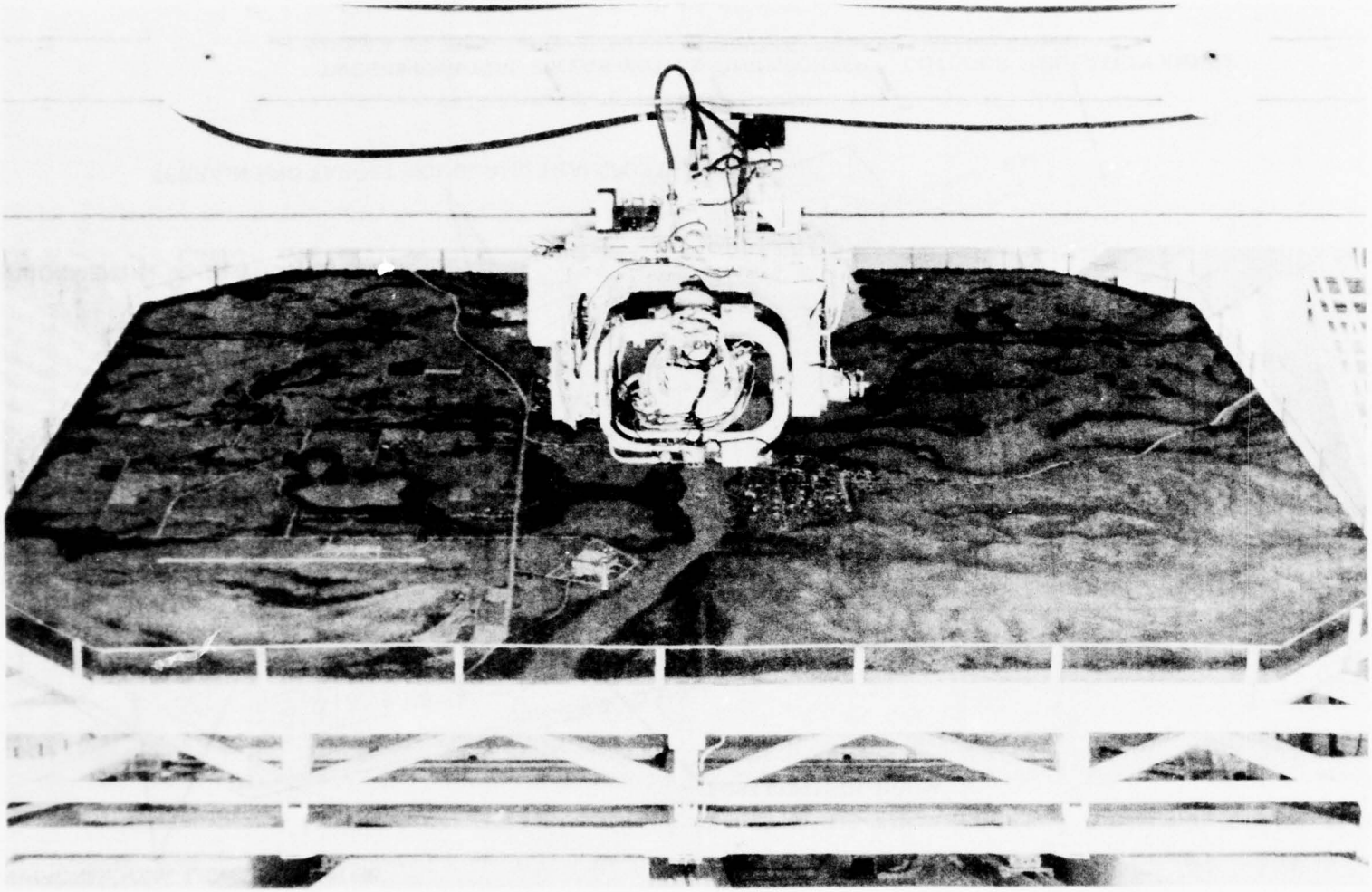

Figure 17. Three-axis mount and terrain model.

E. Implementation

Major EOSS components used in the simulation are the Applied Dynamics AD-4 analog computer, DEC PDP 11/20 digital computer, the three-axis camera mount, and the terrain and target model. Using results from analytical studies, the missile airframe dynamics are modeled on the analog computer. Interfaced with the analog computer is the ground station equipment which includes the video monitor, command console, and decoder as shown in Figure 18. The TV camera is mounted on the three-axis camera mount (Figures 19 and 20). Trajectory data were collected using X-Y plotters and reduced on a digital computer to obtain miss distance information. Figure 21 presents a schematical representation of the simulation.

The operator controls the analog computer via a command console. The airframe motion is transformed into camera fixed coordinates, and this information is used to drive the various EOSS components. The gimbaled camera mount is capable of simulating the pitch, yaw, and roll motion of the camera and is attached to the two-dimensional linear transporter which moves vertically and laterally to simulate the translational terms. Longitudinal translation is simulated by moving the terrain model toward the camera mount.

In the normal operation of the EOSS, the various laboratory components are electrically and physically restrained from making contact. These limits, in turn, impose restrictions on terminal trajectory calculations. Typically, for targets placed upon the terrain model, the point of closest approach between the camera mount and target is approximately 1 m. Considering the fact that the targets on the terrain model are scaled at either 600:1 or 300:1, the closest simulated approach possible using these targets would be 300 m. For low velocity vehicles, such as a mini-RPV, the use of such targets prevents the collection of useful terminal trajectory data. Because of this, the RPV simulation was conducted with a target scaled at 24:1 and made of soft material to prevent damage in case of contact. Further, this target was elevated above the terrain model to allow closer camera and target proximity. With this arrangement, it was possible to obtain final separations of approximately 0.33 m, thereby producing simulated separations of approximately 7.5 m and making it possible to obtain accurate target impact information.

The actual system hardware used in the simulation consisted of an Westinghouse TV camera, a Conrac TV monitor, and a Kraft 6-channel digital proportional radio control encoder. The TV camera presents no interfacing

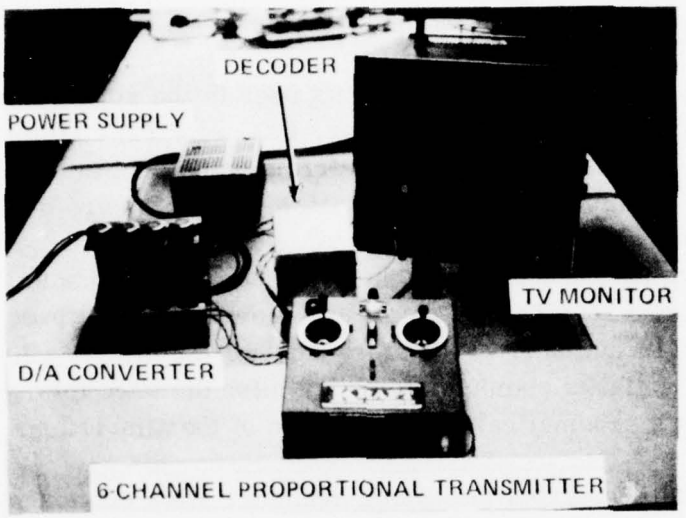

Figure 18. Ground station control.

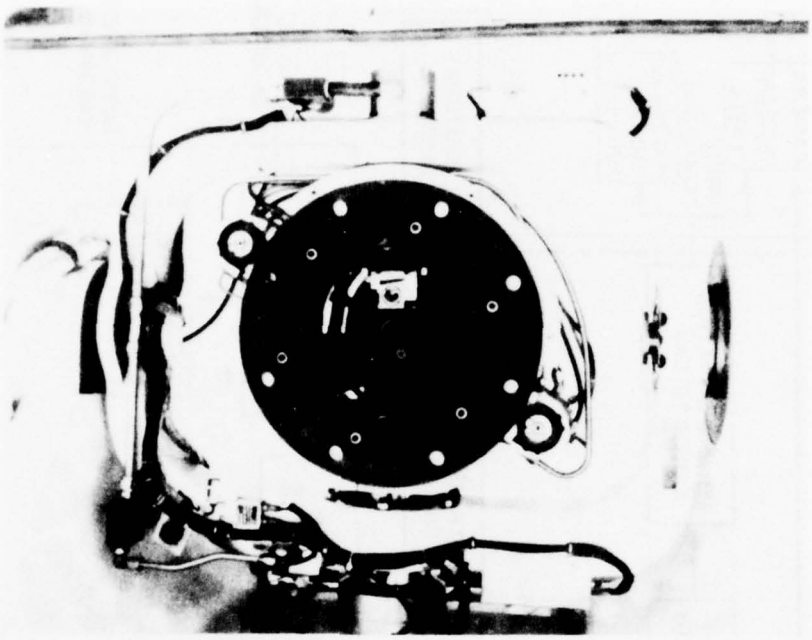

Figure 19. EOSS TV camera mount.

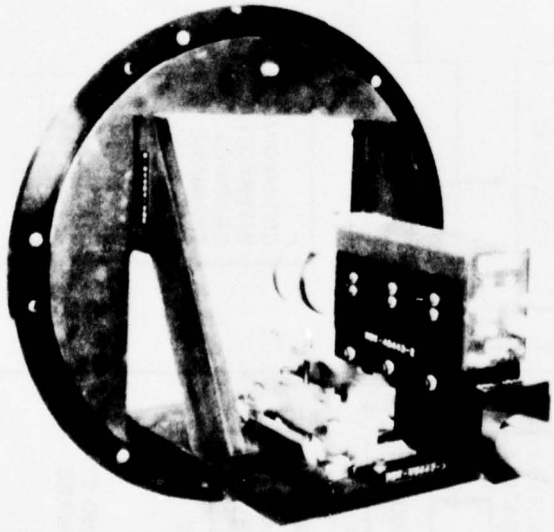

Figure 20. EOSS TV camera mount (rear view).

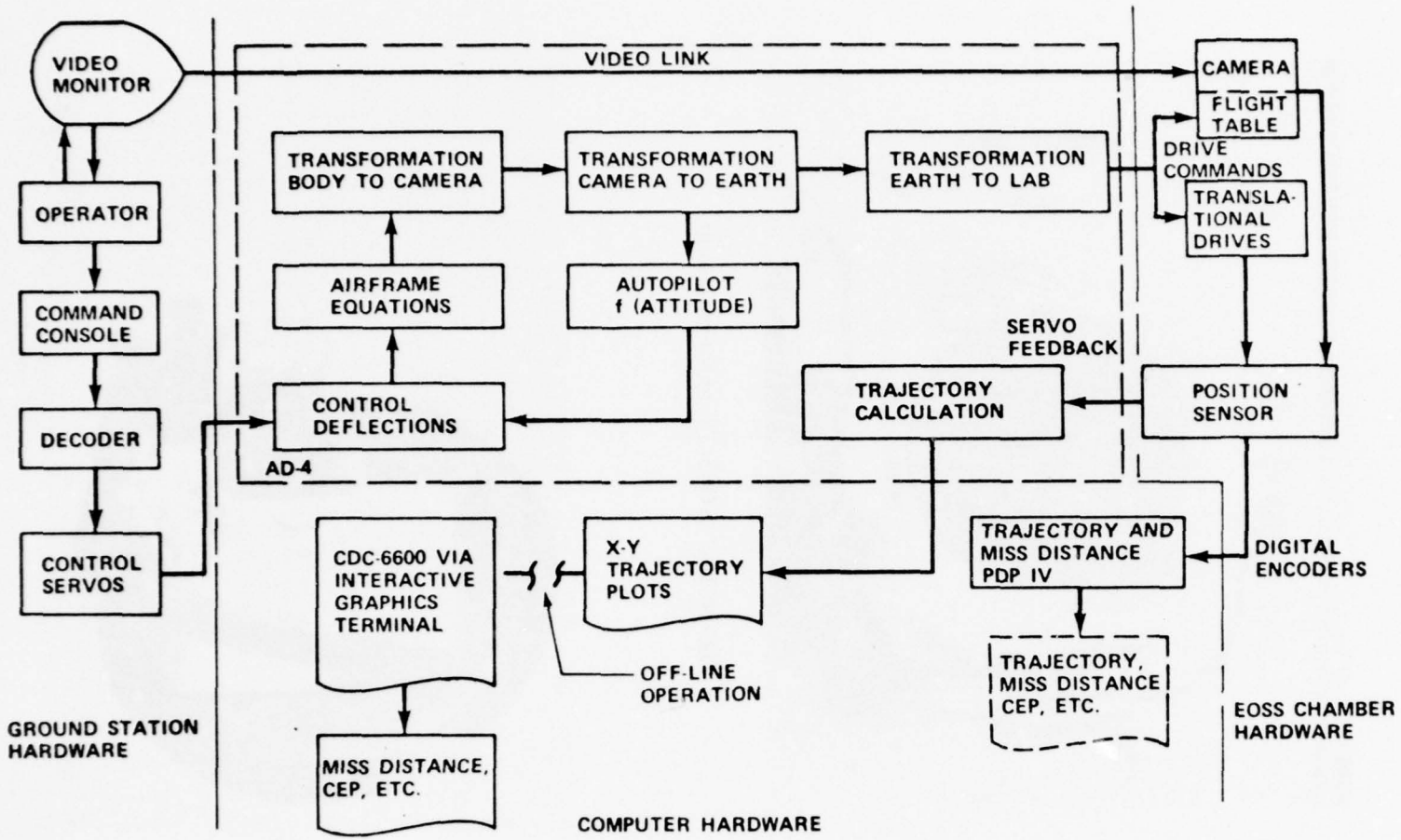

Figure 21. Mini-RPV simulation.

problems because it is not in the simulator loop and is directly connected to the TV monitor. Table 4 presents the characteristics of the TV camera used in this study.

TABLE 4. TV CAMERA DATA

Sensor Type (Westinghouse WTC-25)	
Beam focus	Magnetic
Beam deflection	Magnetic
Physical Data	
Size	2.2 × 3.0 × 5.4 in.
Weight (less lens)	1.2 lb
Electronics	
Input voltage	12 ± 1 V
Input power	7 W at 12 V
Scanning system	525 lines
	30 frames/sec
Interface	2:1
Video bandwidth	7 MHz
Performance	
Maximum resolution	550 lines
Signal-to-noise ratio at 4 fc faceplate I11	40 dB

The radio control system was modified to eliminate the RF up link. The transmitted encoder output is fed into the receiver decoder to provide a pulse directly into the servo. The pulse width is proportional to the control stick position.

Each servo circuit compares the width of the pulse coming from the decoder with an internally generated pulse whose width is determined by servo position. If there is a difference between these two pulses, the servo changes position until the internally generated pulse matches the pulse from the decoder.

In the RPV, this servo position is mechanically converted into a control surface deflection. The analog computer used in the simulation, however, needs a voltage input and so the servos used in the simulation are mechanically coupled to potentiometers. The servo position is thus translated into a positive or negative voltage which the analog computer interprets as a deflection.

This method of control, while more complex than direct coupling of the transmitter potentiometers to the analog computer, utilizes most of the flight hardware and, thus, simulates servo lag, nonlinearities, and other items which contribute to the "feel" of the controls in the actual RPV.

The studies involving unmanned guidance schemes used the same simulation model previously described but modified in the control section. In these studies a television seeker (TVS) was used.

III. SIMULATION RESULTS

A. Manually Controlled Terminal Trajectory

In evaluating the RPV performance, the simulation effort was limited to the terminal trajectory where performance is most critical. The nominal trajectory represented an engagement with missile-target separations of 420 m in range, 120 m in altitude, and with the cross-range separation arbitrarily varied between flights. In all cases, the pilot had visual contact with the target when the engagement started. The trajectory information was plotted on X-Y plotters, and miss distance information was then extracted off-line.

The approach taken in the simulation was to perform a parametric study about configuration C0 and observe circular error probability (CEP), defined as a circle in which 50% of the flights will impact, for a group of flights (usually 10 or more) under the same initial conditions. This parametric study included variations in camera depression angle (necessary for horizon reference), roll autopilot gain, aerodynamic configuration, and control gain. In addition, qualitative results were obtained for control station modifications.

The major problem identified for conventional bank-to-turn configurations, such as C0, involved camera depression angle and vehicle roll. The problem arises from the fact that with the camera aligned off the principle (roll) vehicle axis, any induced roll increases the probability that the target will leave the TV FOV because the camera will experience a yawing or sweeping motion as well as rolling.

In investigating this parameter, two experienced pilots were used and the data statistically summed to obtain vehicle performance as shown in Figure 22. These data indicate that the CEP is not significantly influenced by camera depression angle for angles greater than 5°. The deterioration of vehicle performance observed for the camera aligned with the principle axis results from the fact that the pilot must aim the nose down to see the target. This maneuver requires continual course correction, resulting in the target leaving the FOV. The periodic loss of target makes interception extremely difficult, and, in fact, neither pilot hit the target under this condition.

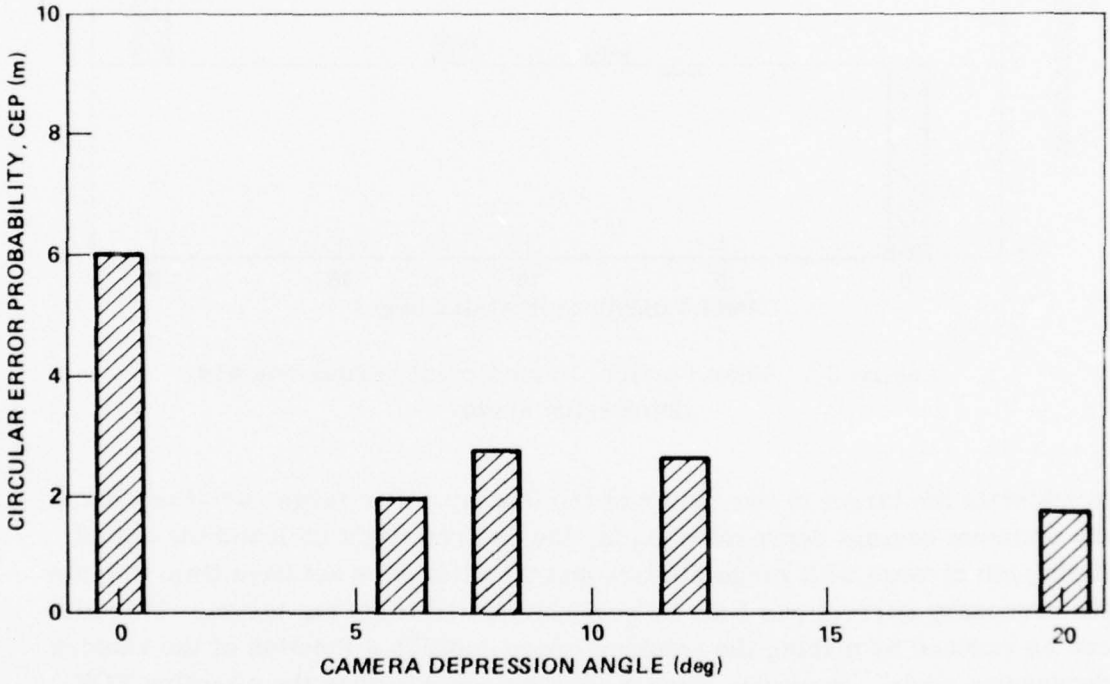

Figure 22. Effect on CEP of variations in camera depression angle.

Vehicle performance cannot be measured by CEP alone. Another important parameter involves the mean impact coordinates. In the case of camera depression angle, the vertical mean impact point becomes important as shown in Figure 23. In the simulation effort the pilot had the benefit of a fixed tracking cross centered on the TV monitor. With this arrangement the pilot tries

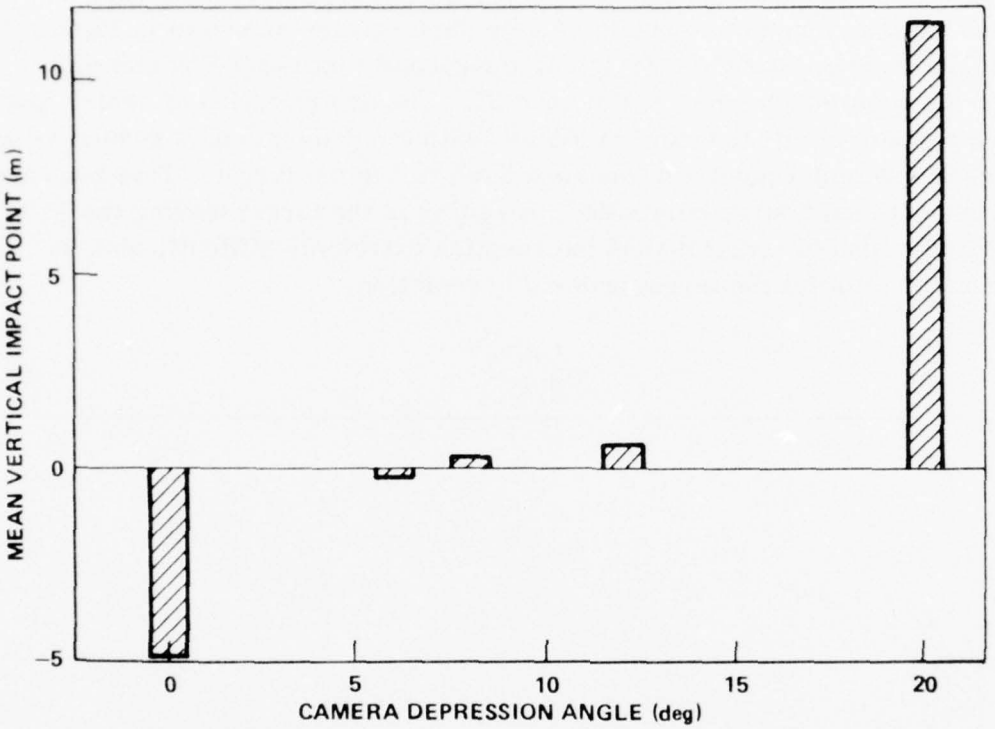

Figure 23. Mean vertical impact point versus camera depression angle.

to maintain the target in the center of the display. For large variations about the optimum camera depression angle, the desired flight path and the actual flight path diverge with range closure and the pilot does not have time to make the necessary corrections once he realizes he will miss the target. This bias can be reduced by making the tracking cross position a function of the camera depression angle. However, such a solution could reduce the effective FOV in certain engagement situations. Figures 22 and 23 indicate that a camera depression angle of from 6 to 12° would be adequate from a miss distance standpoint. Twelve (12) degrees was chosen because it also is optimum for horizon reference.

Even with the optimum camera depression angle, miss distance performance is inadequate and ways to minimize it were needed. An obvious parameter to vary in this regard is roll autopilot gain. The same pilots were used and the

system performance is shown in Figure 24. The data indicate that a roll autopilot improves system performance but is fairly insensitive to gain. It can be concluded then that the autopilot alone cannot provide the needed roll stabilization. The reason for this is that the autopilot, regardless of gain, does not prevent the temporary loss of target during certain banking maneuvers. Also, if the autopilot becomes too effective, the resistance to desired maneuvers will degrade performance.

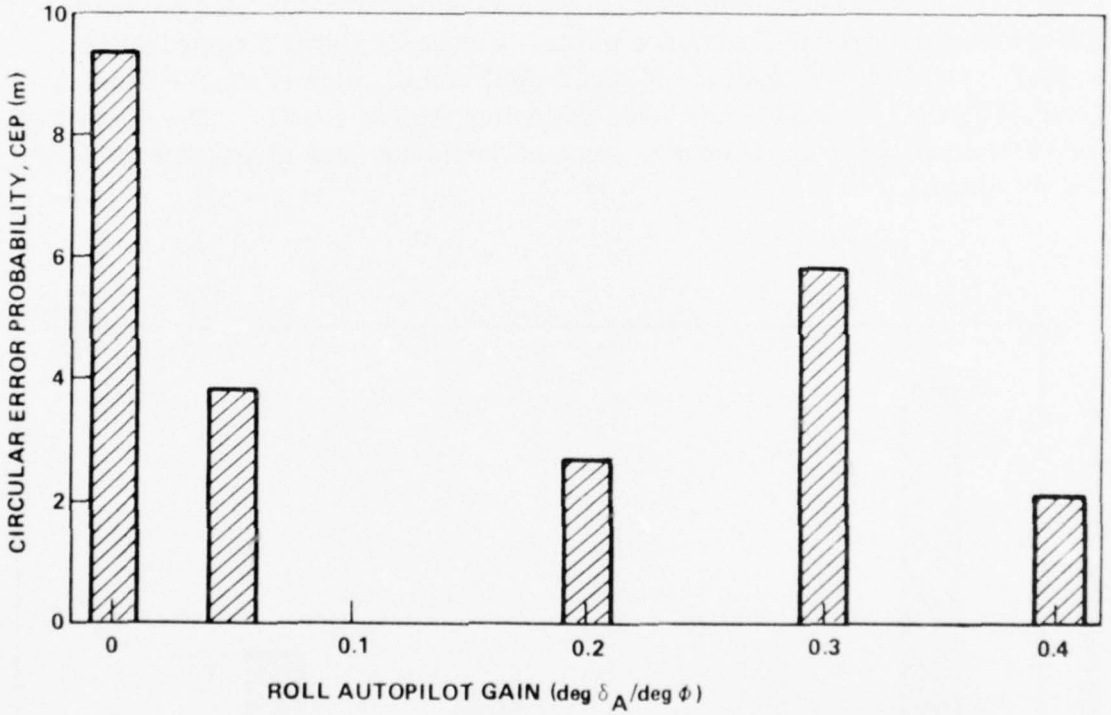

Figure 24. System performance versus roll autopilot gain.

The results at this point indicated the need to roll stabilize the TV image presented to the pilot. One way would be to stabilize the TV camera. Another way, and the one selected in the study, involves the roll stabilization of the entire airframe. This involved the simulation of four configurations that were variations of configuration C0 by the inclusion of vertical wings as shown in Figure 14. These changes resulted in a more effective rudder that provides translational movement with minimal vehicle roll.

The simulation of these configurations was conducted with an autopilot gain of 0.2 deg δ_A/deg ϕ and a camera depression angle of 12°. Additionally, the control function was changed to a single stick configuration (i.e., with the rudder and elevator on one stick). All flights of configurations C1 through C4 were conducted with the ailerons in the autopilot loop only.

Comparative performance data, as measured by CEP, are shown in Figure 25. The data are based on experienced pilots at the controls and show an average improvement by a factor of 2 for the roll stabilized configurations. Configuration C1, which performed 2.4 times better than C0, was chosen for further studies involving untrained pilots. Figure 26 shows a comparative impact array obtained from simulation. Roll stabilization of the TV camera alone, although not simulated, could yield comparable results. The pilots task would be more difficult, however, since he would not have direct control over the TV image.

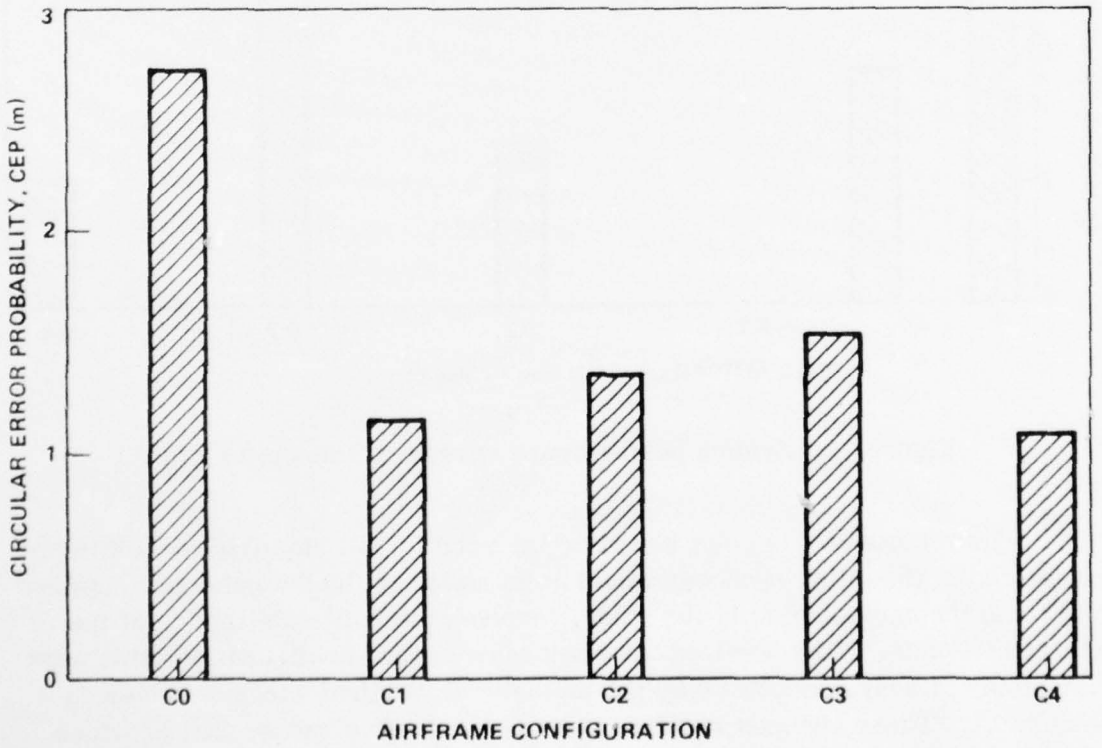

Figure 25. Comparative performance of RPV aerodynamic configurations.

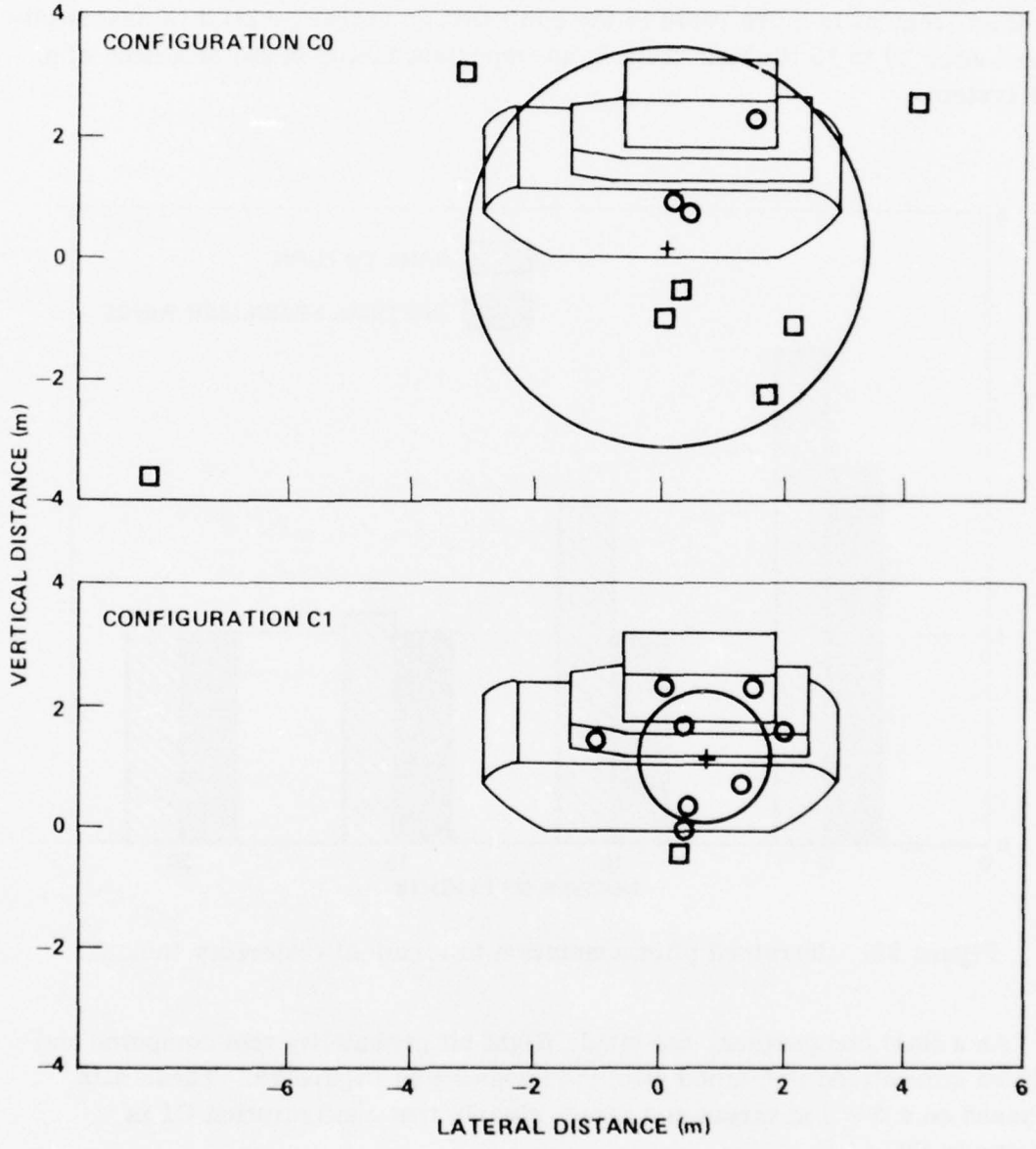

Figure 26. Typical target impact points for a trained pilot.

Another important factor in airframe selection is the pilot's ability to adapt to the flight task. It is shown in Figure 27 that not only can the pilot perform better after a limited number of flights with configuration C1, but also improvement is more rapid to the point that an untrained pilot is essentially trained after 10 to 15 flights. This is an important factor in the selection of a final system.

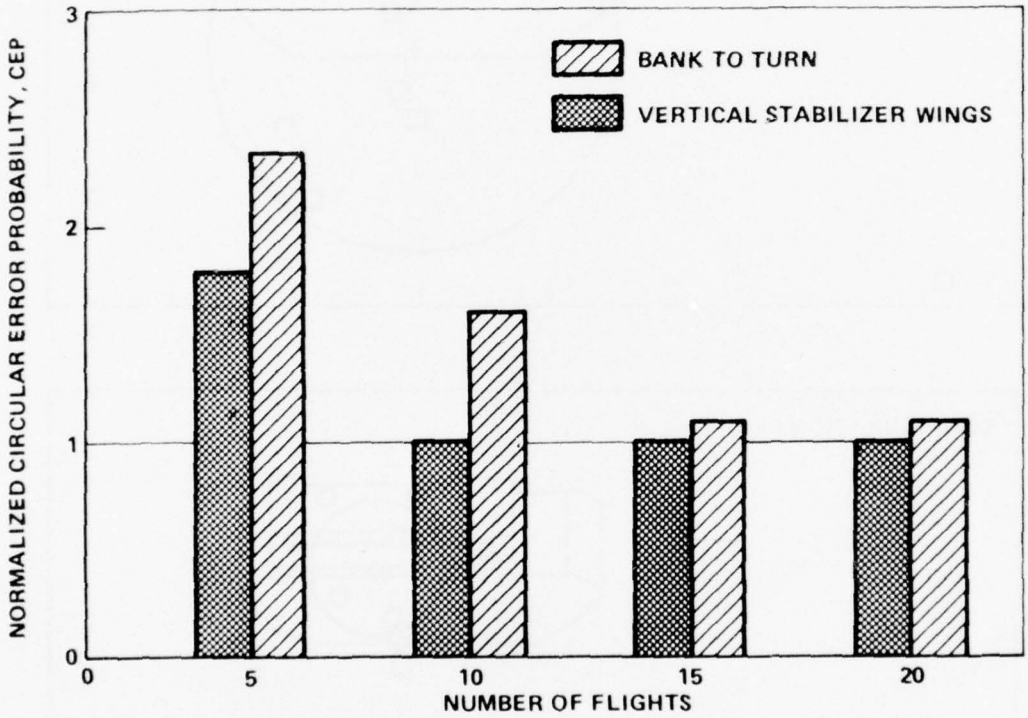

Figure 27. Untrained pilot adaptation to terminal trajectory task.

As a final comparison, the single flight hit probability was computed and is shown normalized to trained pilot performance in Figure 28. These data are based on a 3×3 m target and show clearly that configuration C1 is superior to C0.

In addition to the preceding, limited results were obtained for other system parameter changes. These studies involved control system variations and constant velocity surface winds. A total of 30 flights were made with the aileron control gain varied by a factor of 2 without any significant performance change.

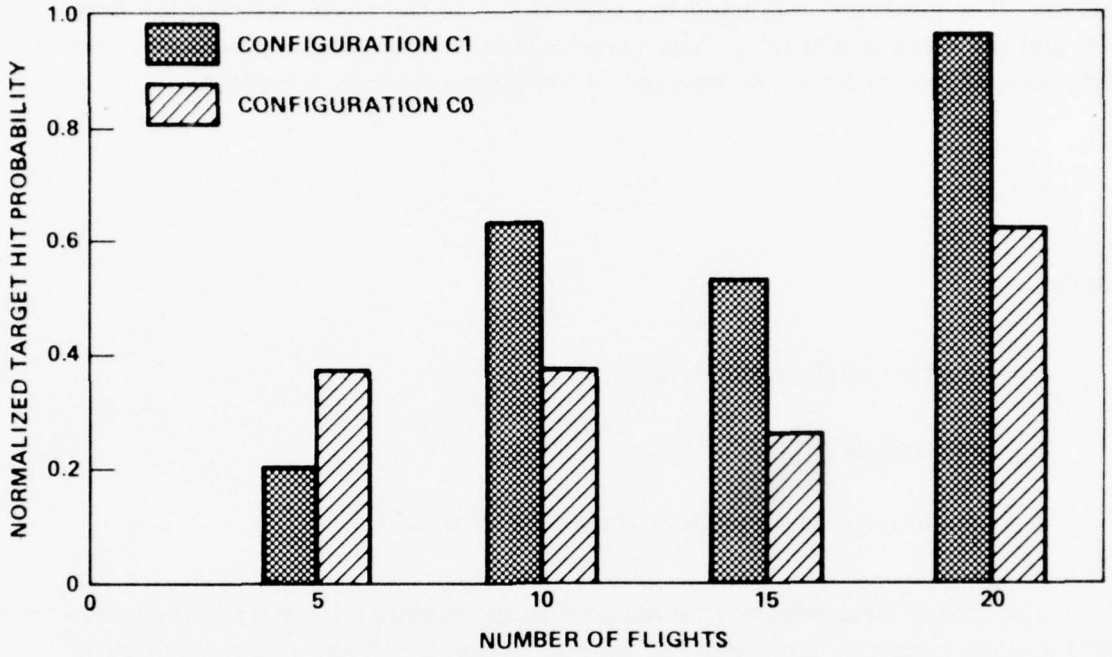

Figure 28. Comparative single flight hit probability for untrained pilots normalized to trained pilot performance (3 × 3 m target).

Qualitative results were taken involving a single stick control station and the observation of all pilots indicated that it made their task simpler. A total of 76 flights using configuration C0 were made to determine the effects of wind on target impact performance. The wind velocity in all cases was a constant 3 m/ sec and was varied in direction. The results show that the CEP performance deteriorates by approximately 10% from the no wind cases. Since the change was small, no runs were made using configuration C1.

B. Unmanned Terminal Guidance

To fully evaluate an attack mini-RPV concept, it is necessary to consider terminal guidance schemes other than man-controlled. Three fundamental guidance schemes were considered: (1) attitude pursuit using a strap-down (body-fixed) TV seeker, (2) proportional navigation using a strap-down TV seeker, and (3) proportional navigation using a stabilized TV seeker. The first two candidates were considered because of potential cost benefits, and the stabilized concept was considered for accuracy comparison purposes.

An attitude pursuit control scheme utilizes a strap-down or body-fixed seeker. The guidance command is proportional to the angle between the true LOS and the missile attitude. The vehicle is turned to point the seeker boresight toward the target. The concept is presented mathematically as

$$\delta = \kappa\epsilon$$

where

δ = control surface deflection

κ = control gain

ϵ = angle between vehicle attitude and boresight.

The major weakness of this scheme is the inability to correct for boresight errors resulting from wind or moving targets. Results show that for a reasonable control gain that the crosswind sensitivity is approximately 1-m miss distance per 1-m/sec wind velocity. The sensitivity to moving targets is roughly the same. Considering these errors and other system errors as well, it is not unreasonable to expect a CEP of from 10 to 20 m for this concept. Therefore, it is reasonable to assume that an attitude pursuit scheme alone cannot provide the required performance for an attack mini-RPV. The possibility does exist, however, for augmenting a manually controlled system with an attitude pursuit scheme.

In proportional navigation schemes the vehicle flight path turning rate ($\dot{\gamma}_m$) is proportional to the LOS rate ($\dot{\sigma}$). Implementation involves making the control surface deflection proportional to $\dot{\sigma}$; i.e.,

$$\delta = \kappa\dot{\sigma} \quad .$$

Usually, proportional navigation schemes are mechanized by mounting a sensor on a 2DOF inertially stabilized platform. In this manner the seeker can lock on and track a target independent of vehicle body motion. Another possible mechanization involves the use of a strap-down seeker. In this case,

the boresight angular error, ϵ, is differentiated and summed with the vehicle body rate $\dot{\phi}_m$ (obtained from on-board rate sensors) to provide an approximate LOS rate, $\dot{\sigma}$; i.e.,

$$\dot{\sigma} \sim \dot{\epsilon} - \dot{\phi}_m \quad .$$

Figure 29 shows a simplified block diagram of the schemes.

These two concepts were investigated for both configurations C0 and C1 using a TVS. When the TVS is used in the stabilized mode, the LOS rate is obtained directly from the hardware. To simulate the strap-down concept, the seeker was left in the caged mode and the boresight error, also a hardware output, was differentiated and summed with the ideal body rates from the dynamic simulation. The results revealed the following:

1) The performance of both schemes is independent of airframe configuration for the range of trajectories considered.

2) Both schemes can reasonably yield a CEP of approximately 1.0 m in the absence of large, impulse disturbances.

3) The proportional navigation scheme using a strap-down seeker can experience loss of lock for impulse disturbances such as wind gust. This results from body rates of a magnitude exceeding the seeker tracking rate capability.

Although more work needs to be done in this area, the general conclusion at this point is that a strap-down seeker concept cannot perform to acceptable limits in the mini-RPV attack role but may be useful as augmentation for manned control. Of course, the stabilized seeker performs satisfactorily but has the disadvantage of being costly.

IV. SIMULATION VALIDATION AND FLIGHT TESTS

Two methods were used in establishing the validity of the simulation. The first method consisted of a qualitative comparison of the simulation and the vehicle in flight as viewed by pilots who had considerable experience.

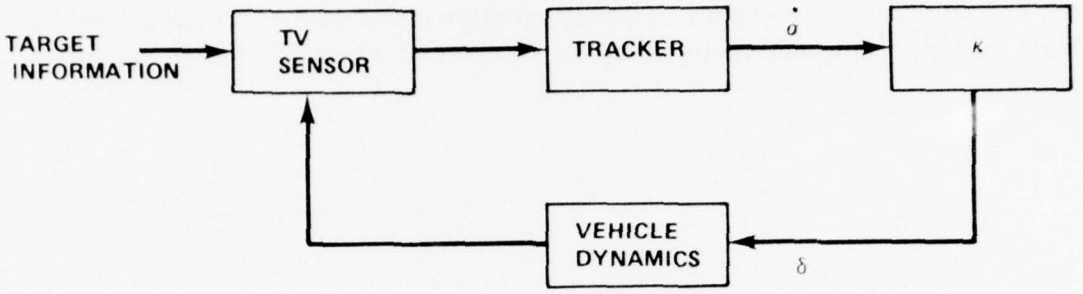

STABLIZED SEEKER

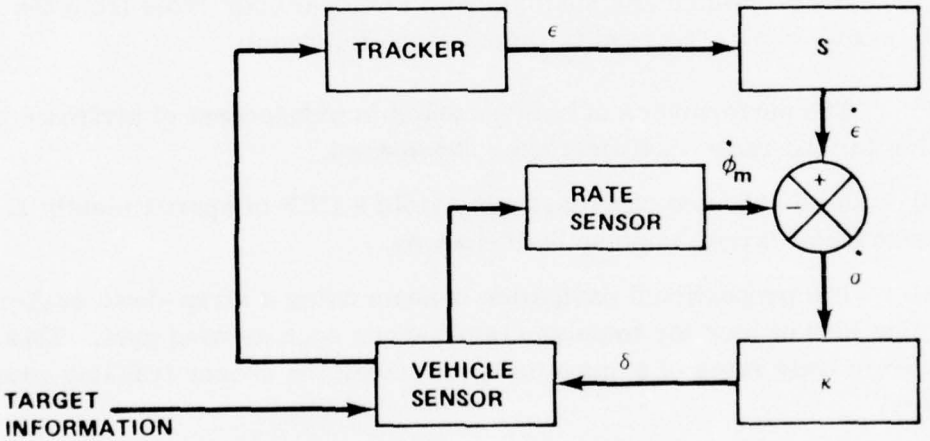

STRAP–DOWN SEEKER

Figure 29. Proportional navigation concepts.

These pilots all agreed that the simulation response was identical to the vehicle response when viewed through the TV monitor. The primary validation procedure, however, consisted of a series of flight tests.

The target used for the test was a standard neoprene weather balloon inflated with helium to a nominal 2-m diameter. It was tethered at an altitude of approximately 10 m by five cotton strings set in pyramidal configuration for

stability as shown in Figure 30. Data were obtained from two 70 mm cameras set at right angles and was reduced by measuring the distance from the tail of the aircraft to the center of the balloon at the point of closest approach. Figure 31 shows a typical flight.

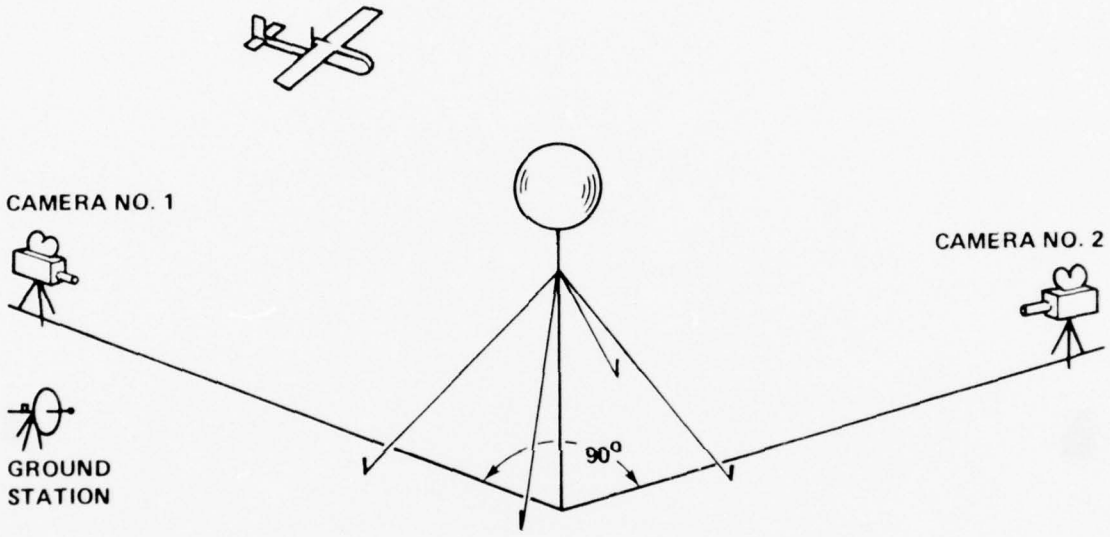

Figure 30. Flight test layout.

The piloting procedure used consisted of a visual pilot and a TV pilot. The TV pilot's transmitter generated a modulation signal and applied it to an outgoing RF carrier wave. The transmitters were wired together and the visual pilot had control over which modulation signal was fed through to the RF carrier. In this manner the visual pilot could give control to the TV pilot or regain control himself if necessary.

Flight tests were made using configuration C0 in May, July, and August of 1975. A total of five flights encompassing 38 target passes were made with data being returned on 20 of the passes. Data camera problems resulted in the loss of data on the remaining passes. A complete summary of the tests is given in Table 5.

The pilots used in the flight test were the same as those experienced pilots used in the simulation. Comparative results from these tests show that the pilots had a cumulative CEP of 6 m in the simulation and 7.9 m for the flights. Factors that explain the difference in the results include the following:

Figure 31. Typical flight test.

TABLE 5. TEST FLIGHTS

Date	Flight No. *	Data Passes	TV Pilot	Weather Conditions	Comments
28 May 1975	82	None	12,13	87°F, wind from south at 8 kn, 90% humidity.	Orientation flight for pilots 12 and 13. No balloon, 4 launches, 1 flight.
29 May 1975	83,84,85, 86,87	24**	12,13	85°F, wind from south at 8 kn.	Passes 1, 2, 3, and 6 with outside operator, passes 8 and 9 not on film. Data returned on 14 passes.
24 July 1975	88,89	None	11	88°F, cloudy, no wind, local thundershowers, 90% humidity.	Orientation flights for pilot 11. No balloon.
25 July 1975	90	None	-	90°F, cloudy, no wind, local thundershowers, 90 to 95% humidity.	2 launches, no flights.
30 July 1975	91,92	8	11	85°F, cloudy, wind from east at 10 kn gusting to 25, 80% humidity.	No balloon for flight 91. Moderate turbulence. Pass 8 not on film (camera failure).

TABLE 5. (Concluded)

Date	Flight No.*	Data Passes	TV Pilot	Weather Conditions	Comments
1 August 1975	93	6	11	80°F, partly cloudy, wind from east at 10 kn gusting to 25, 75% humidity.	Heavy turbulence. Pass 5 hit balloon string. Data returned.

*Flight number refers to total flight number of RPV C0 as recorded in log.
**Data passes occurred on flights 85, 86, and 87.

1) The test sample size was 20 flights and the corresponding simulation sample size was 220.

2) Wind gust up to 13 m/sec were evident in some of the flights, and the simulation included constant winds only.

3) A reluctance on the part of both the visual pilot and the TV pilot to engage the target in the vertical coordinate. This is indicated by the fact that the mean vertical impact point for the flight test was 5.5 m, whereas the corresponding value from the simulation was 0.6 m.

The original test plan called for flight testing configuration C1. This configuration has been fabricated but funding cuts caused the cancellation of this effort. However, with the data collected on configuration C0, it is believed that the simulation is a valid representation of the actual vehicle.

V. COMPUTER SIMULATION OF HUMAN PERFORMANCE IN CONTROLLING AN ATTACK RPV

A. Introduction

In the previous sections, the results of flights of a prototype attack RPV and simulation of an attack RPV in the electrooptical simulation facility with human operators "in-the-loop" were presented. This section will present a method for all digital simulation; that is, in addition to the RPV, the human operator is simulated. The effort is incomplete at this time; therefore, emphasis will be upon the method and not results. This may appear to be a rather distant "related topic" but one, hopefully, that may prove interesting.

B. Optimal Control Man-Model

During the past several decades there has been considerable effort to model-man as a controller, mainly to study aircraft handling. The most successful was the frequency domain, describing function approach [8,9], but it has certain limitations [8]. In the sixties another approach using state variables and optimal control theory showed great promise in overcoming some of the limitations of the describing function approach. In particular, the optimal control model provides, in addition to the mean time histories, the (co) variance time histories, multiple input (displays) and output, and is adaptive to the task. Of course, the ensemble statistics are of particular interest in evaluating a system's effectiveness.

The model used here is the Baron-Kleinman-Levison Model [9,10], also known as the BBN (Bolt, Beranek, and Newman, Inc.) or Optimal Control Model (OCM). The basic assumption is that the well-trained well-motivated human operator behaves in an optimal manner, subject to his inherent limitations and the requirements of the control task [10]. The model based upon this assumption has been validated [10,11]. As humans, it is pleasing to know we do some things optimally.

The model utilizes linear-quadratic-Gaussian estimation and control theory. The details of the model are well documented [10 through 13] and time does not permit their review here. But only a brief outline of the model is required to follow the application to the attack RPV problem.

How the various inherent human limitations are introduced into the model may be seen in Figure 32. The observation, $y(t)$, is subjected to observation noise, -20 dB, and a "perceptual" time delay, $\tau \sim 0.2$ sec. An estimate of the delayed state of the system, $\hat{x}(t - \tau)$, is reconstructed by a Kalman filter and brought up to date by the predictor. Then the optimal control, $u_c(t)$, is computed. The control is then subjected to motor noise, -25 dB, and a "neuromuscular" time delay, $\tau_N \sim 0.1$ sec. Actually the neuromuscular time delay is implicit in that it is introduced by weighing on the control rate in the performance index (cost functional). That is, the weighing on control rate is adjusted so that the computed $\tau_N = 0.1$ sec or some value in agreement with the test data being analyzed.

That the inherent limitations so modeled remain invariant, or nearly so, across a wide range of system dynamics in validation test is the power of the model. Of course, the estimator, predictor, and gains are dependent upon the systems dynamics and the task; therein lies the adaptability of the model.

The plant is defined by an equation of state,

$$\dot{x} = Ax + Bu + En$$

and the display by an observation equation,

$$y = Cx + Du$$

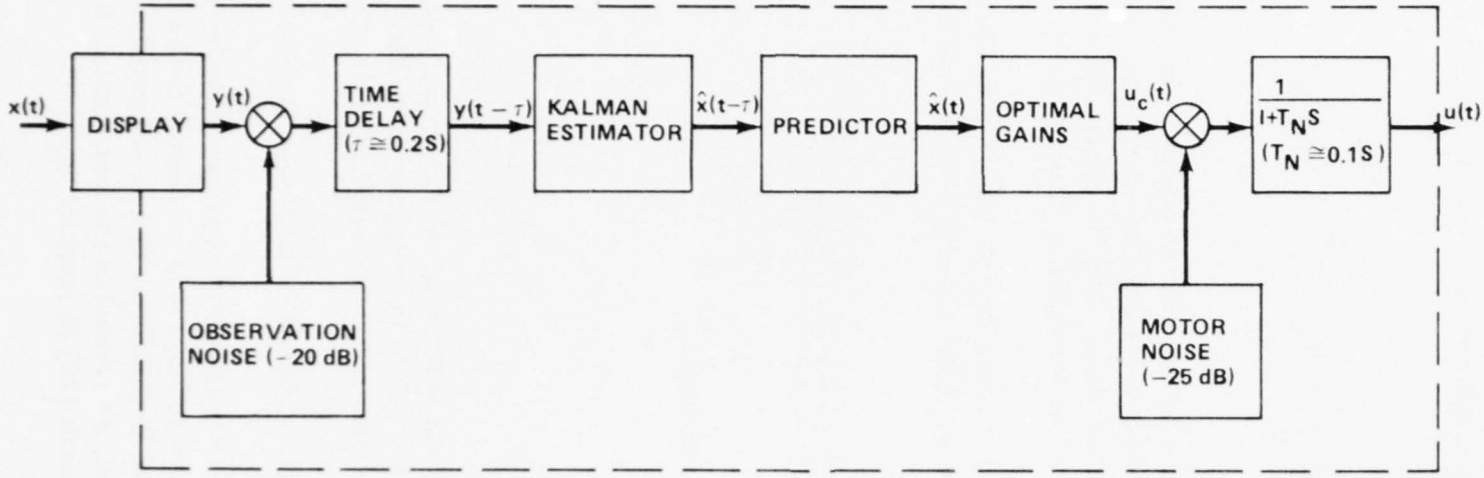

Figure 32. Man-model.

The task requirements are defined by a cost functional or performance index

$$J(t_f) = \frac{1}{2} x^T F x + \frac{1}{2} \int_0^{t_f} x^T Q_x x + y^T Q_y y + u^T R_u u + \dot{u}^T R_{\dot{u}} \dot{u} \, dt \quad .$$

These equations supply the information to compute the optimal filter and control gains. If the control gains are not to be constant, they must be integrated backwards in time from the final time. The "final" condition would be matrix F. The filter gains are computed forwards in time and present no difficulty.

Those familiar with modern control theory may have found the cost functional a bit strange. The problem actually being solved has the state equation

$$\begin{pmatrix} \dot{x} \\ \dot{u} \end{pmatrix} = \left(\begin{array}{c|c} A & B \\ \hline 0 & 0 \end{array}\right) \begin{pmatrix} x \\ u \end{pmatrix} + \begin{pmatrix} 0 \\ 1 \end{pmatrix} \dot{u} + \begin{pmatrix} E \\ 0 \end{pmatrix} n$$

and the display observation equation,

$$y = (C \mid D) \begin{pmatrix} x \\ u \end{pmatrix} \quad .$$

These manipulations and the solution of the matrix Riccati equations for the control and filter gains are left to the computer program. The engineer's problem is to supply the input matricies which describe the plant and the task.

C. Linearized Equations of Motion for an Attack RPV

Since the man-model has been formulated using linear-quadratic-Gaussian control theory, it is necessary to linearize the systems equations of motion. The linearization of aircraft equations of motion is well treated in Kolk [14], and, as related to the man-model, the linearization in Kleinman and Killingsworth [15] is instructive.

The configuration C0 requires roll to turn, and the resulting aircraft equations are nonlinear which present difficulties in modeling. Fortunately, configuration C1 proved to be easier to fly and more accurate. Fortunate because the equations for C1 are easily linearized (Figure 33).

The major difference between the flight test and the EOSS simulation was the presence of gust in the flight test. It was therefore decided to use the man-model to study the effects of gust on performance. This requires a linear gust model

D. Dryden Wind Gust Model

The principle external disturbance acting on the RPV is wind turbulence or gust. The Dryden model [16] is a first order Markov process with power spectral density

$$\Phi(\omega) = 2\sigma_g^2 \left(\frac{V_0}{L}\right)\left(\frac{1}{\left(\frac{V_0}{L}\right)^2 + \omega^2}\right)$$

where

σ_g^2 = mean-square gust velocity

V_0 = equivalent air speed

ω = frequency.

L = scale turbulence.

The autocorrelation function and correlation time (1/e point) are

$$\phi(\tau) = \sigma_g^2 e^{-\frac{V_0}{L}(\tau)}$$

$$\begin{pmatrix} \dot{r} \\ \dot{\psi} \\ \dot{\beta} \\ \dot{y} \end{pmatrix} = \begin{pmatrix} -QSb^2 C_{N_r} & 0 & \dfrac{QSb\, C_{N_\beta}}{I_z} & 0 \\ 1 & 0 & 0 & 0 \\ -1 & 0 & \dfrac{-QS\, C_{y_\beta}}{mV} & 0 \\ 0 & V & V & 0 \end{pmatrix} \begin{pmatrix} r \\ \psi \\ \beta \\ y \end{pmatrix} + \begin{pmatrix} \dfrac{QSb\, C_{N_{\delta_r}}}{I_z} \\ 0 \\ \dfrac{-QS\, C_{y_{\delta_r}}}{mV} \\ 0 \end{pmatrix} \delta_r$$

$$\dot{x} = \quad A \quad x + B \quad u$$

r = YAW RATE
ψ = YAW PATH ANGLE
β = YAW ANGLE OF ATTACK
y = CROSS RANGE DISPLACEMENT
δ_r = RUDDER DISPLACEMENT
$Q = 1/2\ \rho\ V^2$
$\rho = 1.225\ kg/m^3$
$V = 30\ m/sec$
$I_z = 1.935\ kg\text{–}m^2$
$m = 11.325\ kg$
$S = 0.92903$
$b = 2.438\ m$

$C_{N_r} = 0.114$
$C_{N_\beta} = 0.427$
$C_{N_{\delta_r}} = 0.0555$
$C_{y_\beta} = 1.421$
$C_{y_{\delta_r}} = 0.125$

Figure 33. Simplified linearized yaw RPV equation of motion for C1.

and

$$\frac{L}{V_0} \quad ,$$

respectively.

To obtain a wind filter to shape a unity rms white noise, n,

$$\Phi(\omega) = |\omega_g(j\omega)|^2 = \omega_g(j\omega)\,\omega_g^*(j\omega)$$

where $\omega_y^*(j\omega)$ is the complex conjugate of $\omega_y(j\omega)$, and spectral factorization of $\Phi(\omega)$ yields

$$\Phi(\omega) = \left(\frac{\left(2\frac{V_0}{L}\right)^{1/2}\sigma_g}{\left(\frac{V_0}{L}\right) + j\omega}\right)\left(\frac{\left(2\frac{V_0}{L}\right)^{1/2}\sigma_g}{\left(\frac{V_0}{L}\right) - j\omega}\right) \quad .$$

Replacing $j\omega$ by the Laplace operator, the wind filter is

$$\frac{\omega_g(s)}{n} = \frac{\left(2\frac{V_0}{L}\right)^{1/2}\sigma_g}{\left(\frac{V_0}{L}\right) + s}$$

and the associated first order differential equation is

$$\dot{\omega}_g(t) = -\frac{V_0}{L}\,\omega_g(t) + \sigma_g\left(2\,\frac{V_0}{L}\right)^{1/2} n(t)$$

which is in the form required by the state variable model.

An alternate form [15] which will be used in the model is

$$\beta_g(t) = -\frac{V_0}{L}\,\beta_g(t) + \left(\frac{\sigma_g}{V_0}\right)\left(2\,\frac{V_0}{L}\right)^{1/2} n(t)$$

where $\beta_g(t)$ is the angle of attack created by the wind gust.

E. Observation Matrix

Much of the earlier work in using the man-modeling techniques was in simulating aircraft operating under instrument flight rules (IFR) [10, 11, 12, 14, 15, 16, 17, 18, 19, 20]. In the case of visual flight rules (VFR) it is not as clear what information is available, but the work of Grunwald and Merhav at Technion, Israel [21, 22, 23, 33] has gone a long way in addressing the VFR modeling problem. Their approach is based upon the concepts of J. J. Gibson [24, 25, 26]. Gibson's approach to visual perception is to examine the information which is available from the visual scene; the physiological process of perception is not at issue. The model is based upon the relative motion of textural points in the visual field, that is, "streamers," the velocity vectors of the textural points. An analogy would be the streaks or blur in a time exposure by a moving camera.

The problem treated by Grumwald and Merhav was the horizontal flight of a TV-RPV. The task was to cruise along a road while being subjected to gust disturbances. They utilized the optimal control man-model as the basis of their analysis. For the fixed reticle, the observed angular error in yaw was

$$\epsilon = \frac{y}{D} + \psi \quad .$$

The error rate is

$$\dot{\epsilon} = \frac{V}{D}(\psi + \beta) + \frac{V}{D^2} y + r \quad .$$

The man-model assumes that for analog displays, the rate is also perceived [10]. The "looking distance," D, was constant in their cruise study, which allowed steady-state analysis. It was found that two looking distances were adequate to model human perception in this task [21,22].

In an attack mode of operation the looking distance, $D = D_0 - Vt$, decreases to zero at the final time. The expression ϵ and $\dot{\epsilon}$ would present numerical difficulties near the final time. An observed linear error in yaw

$$E = y + D\psi$$

with error rate

$$\dot{E} = 2V\psi + V\beta + Dr$$

overcomes this difficulty. The Ponzo or railway lines illusion lends support to an observed linear error in that objects of a given angular size are perceived as larger when perceived to be at a greater distance. In the cruise case, the results would be unaffected since

$$E = D\epsilon \quad ;$$

that is, the only difference is one of scaling weighting.

The velocity vector reticle showed improvements in performance for certain RPV configurations [21]. For the velocity reticle, the observed angular error in yaw is

$$\epsilon = \frac{y}{D} + \psi + \beta \quad .$$

For the reasons previously given, we choose for the velocity reticle the observed linear error in yaw

$$E = y + D\psi + D\beta$$

whose error rate is

$$\dot{E} = 2V(\psi + \beta) + \frac{D}{V}\left(-C_{\beta}\beta - C_{u}u\right) \quad .$$

Though the two looking distance model was adequate for modeling free viewing, it is believed a single looking distance is adequate for modeling attack.

F. Cost Functional Performance Index

The state and observation equations describe the human's internal model of the plant. The weighing of the cost functional describes the requirements of the task, that is, what is to be accomplished.

Suppose one controlled to minimize the observed linear error in yaw, E, throughout the attack. Would this be reasonable? For

$$E = 0$$

it follows that

$$0 = y + D\psi \quad .$$

For constant path angle, ψ_0, that is zero control, angle of attack, and yaw rate, the state equations imply

$$\dot{y} = V\psi_0 \quad .$$

Therefore

$$0 = y_0 + V\psi_0 t + (D_0 - Vt)\ \psi_0$$

or

$$y_0 = -D_0\psi_0 \quad .$$

When

$$D = 0$$

it follows that

$$y = 0 \quad .$$

This will be recognized as the conditions for a constant bearing collision course for small angles. The conditions for a constant bearing collision course have been found desirable in air defense and undesirable in sailing.

Therefore, the weighing on the observation would be

$$y^T Q_y y = E^2$$

or

$$Q_y = \begin{pmatrix} 1 & 0 \\ 0 & 0 \end{pmatrix}$$

Alternatively, one could choose to minimize y at the final time, an intercept problem. In this case,

$$x^T F x = y^2 \quad ;$$

that is,

$$F_{yy} = 1 \quad .$$

Intercept control leads to proportional navigation which reduces the LOS rate to achieve a constant bearing collision course [27].

The weighing in the computer program is

$$x^T Q x = x^T \left(Q_x + C^T Q_y C \right) x \quad .$$

The matrix Q is time varying because of the looking distance, D, in the observation matrix, C, is time varying. In most applications of the man-model to date, the gains have been assumed constant or piece-wise constant. The control problem was one of steady-state regulation. This is not possible here because of the time varying cost on the state Q.

The control gains must be computed backwards in time from the time of impact. That a well trained human operator would develop time varying gains seems to be a logical extension of the optimal control man-model. For this reason a time varying man-model computer program was developed [28]. A caveat, this extension of the model has not been validated at this time.

It is planned to incorporate a gust model into the EOSS simulation. According to References 29 and 30, the first order model used here is more appropriate to longitudinal gust and a second order model should be used for lateral and vertical gust. Another approach to simulating turbulence will be found in Reference 31.

The EOSS simulation would allow validation of the time varying RPV man-model discussed here, then the model could be used to seek out areas of sensitivity to be investigated in the EOSS; that is, help design further test.

The model is easily modified to incorporate augmented controls and displays. Also, the model may be used to study operator workload for various configurations [32].

The human operator has been characterized as a "one hertz servo in a ten hertz world." However, the human operator is adaptable and a fantastic information sensor/processor. It is hoped that models such as the optimal control model will allow understanding of his capabilities and limitations and development of systems he may use to full advantage.

The research in biofeedback has shown how little is really known about man's ability to control; another modeling problem of interest, but beyond the scope of this study.

REFERENCES

1. Bailey, H. H., Target Detection Through Visual Recognition: A Quantitative Model, The Rand Corporation, Memo RM 6158 PR, February 1970.

2. Hoerner, S. F., Fluid Dynamic Drag, New Jersey, 1958.

3. Abbott, I. H., von Doerhoff, A. E., and Strivers, L. S., Summary of Airfoil Data, NACA Report 824, 1945.

4. Pope, A. Y., Basic Wing and Airfoil Theory, McGraw Hill Book Co, Inc., New York, 1951.

5. Durand W. F. and Lesley, E. P., Experimental Research on Air Propellers, V, NACA Report 141, 19 .

6. Hill, M. L., Introducing the Electrostatic Autopilot, Johns Hopkins Applied Physics Laboratory, Astronautics and Aeronautics, November 1972.

7. Perkins, Courtland D., and Hage, Robert E., Airplane Performance Stability and Control, John Wiley and Sons, Inc., New York, 1949.

8. Kelley, C. R., Manual and Automatic Control, John Wiley and Sons, New York, 1968.

9. Sheridan, T. B. and Ferrell, W. R., Man-Machine Systems, MIT Press, Cambridge, Massachusetts, 1974.

10. Kleinman, D. L., Baron, S., and Levison, W. H., "A Control Theoretic Approach to Manned-Vehicle System Analysis," IEEE, Vol. AC-16, No. 6, December 1971, pp. 824-832.

11. Kleinman, D. L., Baron, S., and Levison, W. H., "An Optimal Control Model of Human Response," Part I: "Theory and Validation," and Part II: "Prediction of Human Performance in a Complex Task," Automatica, Vol. 6, 1970, pp. 357-369, 371-383.

12. Kleinman, D. L. and Baron, S., "A Control Theoretic Model for Piloted Approach to Landing," Automatica, Vol. 9, 1973, pp. 339-347.

13. Kleinman, D. L. and Baron, S., Manned Vehicle Systems Analysis by Means of Modern Control Theory, NASA CR-1753, June 1971.

14. Kolk, W. R., Modern Flight Dynamics, Prentice Hall, Englewood Cliffs, New Jersey, 1961.

15. Kleinman, D. L. and Killingsworth, W. R., A Predictive Pilot Model for STOL Aircraft Landing, NASA CR-2374, March 1974.

16. Hoffman, W. C., Curry, R. E., Kleinman, D. L., and Hollister, W. M., Display/Control Requirements for VTOL Aircraft, NASA CR-145026, August 1975.

17. Kleinman, D. L., Solving the Optimal Attention Allocation Problem in Manual Control, IEEE, Vol. AC-21, No. 6, December 1976, pp. 813-821.

18. Baron, S. and Levison, W. H., A Manual Control Theory Analysis of Vertical Situation Displays for STOL Aircraft, NASA CR-114620, April 1973.

19. Kleinman, D. L. and Baron, S., Analytic Evaluation of Display Requirements for Approach to Landing, NASA CR-1952, November 1971.

20. Phatak, A., Gupta, N., and Segall, I., Analysis of Controller/System Dynamics for a Remotely Piloted Vehicle Strike Mission, Aerospace Medical Research Laboratory, TR-74-80, Wright-Patterson AFB, September 1974.

21. Grumwald, A. J. and Merhav, S. J., A Study of Display Augmentation Visually Controlled Vehicles, Technion-Israel Institute of Technology, Haifa, Israel, TAE Report No. 284, May 1976.

22. Grumwald, A. J. and Merhav, S. J., Vehicular Control by Visual Field Cues — Model Development and Experimental Validation, Technion-Israel Institute of Technology, Haifa, Israel (also IEEE-SMC-6 (12), December 1976), TAE Report No. 254, July 1975.

23. Grumwald, A. J. and Merhav, S. J., An Analytical Model for Visual Field Control — A Parametric Study, Technion-Israel Institute of Technology, Haifa, Israel, TAE Report No. 217, June 1974.

24. Gibson, J. J., Olum, P., and Rosenblatt, F., "Parallex and Perspective During Aircraft Landings," American Journal of Psychology, Vol. LXVIII, September 1955, pp. 372-385 (AD 102687).

25. Gibson, J. J., The Perception of the Visual World, Houghton Mifflin, Boston, 1950.

26. MacLeod, R. B. and Pick, H. L. Jr. (Editors), Perception: Essays in Honor of James J. Gibson, Cornell University Press, Ithaca, 1974. In Particular Essay 7, Projective Transforms as Determining Visual Space Perception by G. Johansson.

27. Ho, Y. C., Bryson, A. E. Jr., and Baron, S., "Differential Games and Optimal Pursuit-Evasion Strategies," IEEE, Vol. AC-10, No. 4, October 1965, pp. 385-389.

28. Kleinman, D. L., Baron, S., and Berliner, J. E., TIVAR. A Computer Program for Predicting Ensemble Statistics in a Time-Varying Man/Machine Control Task, US Army Missile Command Contract Number DAAH01-76-C-0194 (in publication) (Bolt, Beranek, and Newman, Inc., Report Number 3464, January 1977).

29. Daniels, G. E. (Editor), Terrestrial Environment (Climatic) Criteria Guidelines for Use in Aerospace Vehicle Development, 1973, Revision, NASA TM X-64757, Marshall Space Flight Center, July 5, 1973 (5.3.14 Turbulence Model for Flight Simulation).

30. Luers, J. K., A Model of Wind Shear and Turbulence in the Surface Boundary Layer, NASA CR-2288, July 1973.

31. Fichtl, G. H. and Perlmutter, M., "Nonstationary Atmospheric Boundary-Layer Turbulence Simulation," J. of Aircraft, Vol. 12, No. 8, August 1975, pp. 639-647.

32. Wewerinke, P. H., "Human Operator Workload for Various Control Situations," Tenth Annual Conference on Manual Control, Wright-Patterson AFB, April 9-11, 1974. (Though not referred to here there have been many papers on the optimal control and other man-models in the "Annual Manual" over the past few years).

33. Grunwald, A. J. and Merhav, S. J., Vehicular Control by Visual Field Cues, Technion-Israel Institute of Technology, Haifa, Isreal, TAE Report No. 292, September 1976.

DISTRIBUTION

	No. of copies
Defense Documentation Center Cameron Station Alexandria, VA 22314	12
Commander US Army Materiel and Readiness Command	
Attn: DRCRD	1
DRCDL	1
5001 Eisenhower Avenue Alexandria, VA 22333	
Bolt, Beranek and Newman, Inc.	
Attn: Dr. S. Baron	1
Dr. J. Berliner	1
Dr. D. Kleinman	1
50 Moulton Street Cambridge, MA 02138	
Systems Control, Inc. Attn: Dr. Amil Platak 1801 Page Mill Road Palo Alto, CA 94304	1
MSFC (NASA) Attn: ES82 Dr. Fichtl Marshall Space Flight Center, AL 35812	1
DRSMI-LP, Mr. Voigt	1
DRDMI -X, Dr. McDaniel	1
-T, Dr. Kobler	1
-TDW, R. Dickson	2
-TDD, D. Holder	1
R. Powell	6
-TBD	3
-TI (Record set)	1
(Reference copy)	1

END
10-77

DISTRIBUTION

	No. of copies
Defense Documentation Center Cameron Station Alexandria, VA 22314	12
Commander US Army Materiel and Readiness Command	
Attn: DRCRD	1
DRCDL	1
5001 Eisenhower Avenue Alexandria, VA 22333	
Bolt, Beranek and Newman, Inc.	
Attn: Dr. S. Baron	1
Dr. J. Berliner	1
Dr. D. Kleinman	1
50 Moulton Street Cambridge, MA 02138	
Systems Control, Inc. Attn: Dr. Amil Platak 1801 Page Mill Road Palo Alto, CA 94304	1
MSFC (NASA) Attn: ES82 Dr. Fichtl Marshall Space Flight Center, AL 35812	1
DRSMI-LP, Mr. Voigt	1
DRDMI -X, Dr. McDaniel	1
-T, Dr. Kobler	1
-TDW, R. Dickson	2
-TDD, D. Holder	1
R. Powell	6
-TBD	3
-TI (Record set)	1
(Reference copy)	1